UNIVERSITY OF CALGARY

Storage and Manipulation of Qubits via Controlled Reversible Inhomogeneous Broadening

by

Michael S. Underwood

A THESIS
SUBMITTED TO THE FACULTY OF GRADUATE STUDIES
IN PARTIAL FULFILLMENT OF THE REQUIREMENTS FOR THE
DEGREE OF MASTER OF SCIENCE

DEPARTMENT OF PHYSICS AND ASTRONOMY

CALGARY, ALBERTA

September, 2008

Abstract

A new variation of the so-called CRIB protocol for quantum memory based on *c*ontrolled *r*eversible *i*nhomogeneous *b*roadening is presented. The CRIB protocol is a proposal to allow quantum states of light to be stored in, and later recalled from, the collective state of a solid-state atomic ensemble. An introductory discussion explores the theory of the original protocol, which relies on a hidden time-reversal symmetry in the Maxwell-Bloch equations. This symmetry is then broken here in a controlled fashion, by considering a single storage medium as two spatially-distinct segments when recalling the light. The stored photonic state is recalled from the two segments individually; this results in a superposition state in which the photon has specified probabilities to have left the storage medium at one of two times, either 'early' or 'late'. It is shown that the operations of a beam splitter and phase shifter, the fundamental building blocks of any optical setup, can be implemented in a quantum memory under this new version of the protocol. Motivation for the work is drawn from experimental implementations of quantum key distribution, in particular from the need to perform projective measurements onto certain bases when making use of the protocol due to Bennett and Brasard in 1984. Simulations of the systems described herein were performed; their results are presented, and agree with the theoretical predictions.

Acknowledgements

I would like to thank my parents, Bruce and Joanne, for their continuous and unfailing support through every stage of my life. They taught me the value of critical thinking, encouraged an active imagination, and showed me that problems can be looked at as challenges, and their solutions as rewards unto themselves.

I would also like to thank my wife Katie, whose confidence and support have been invaluable to me throughout my studies. In particular I could not have finished this document the same week we got married without the enourmous effort which she put in to the planning of our wedding, along with my parents-in-law, Debbie and Harold.

Finally I would like to thank my supervisors, Peter and Wolfgang, for their guidance, dedication, expertise, and advice.

Table of Contents

List of Tables

List of Figures

Chapter 1

Introduction

1.1 Quantum key distribution

In 1984 at a conference in Bangalore, Charles Bennett and Gilles Brassard presented a protocol which allows the uncertainty principle of quantum mechanics to be exploited in such a way as to distribute a cryptographic key between two parties [BB84]. What makes this key distribution protocol unique is that it guarantees no third party can gain information about the key without advertising their eavesdropping attempt to the original two. Furthermore, the two communicating parties require only a small amount of shared secret information in order to prove that they are who they claim to be; besides this initial authentication they can communicate large volumes of data with absolute security. Within five years Bennett and Brassard proclaimed "The dawn of a new era for quantum cryptography: The experimental prototype is working!" [BB89]. By 1991, Bennett, Brassard, and others had implemented this protocol, now commonly referred to as 'BB84', to distill a secret key between two fictional parties simulated by the same computer, over a free-space quantum channel 32 cm long [BBB$^+$92]. They also predicted that existing optical fibres could extend the length of the channel to "at least several kilometers."

Also in 1991, Artur Ekert, then working independently, extended the proposal of Bennett and Brassard by making use of the Einstein-Podolsky-Rosen paradox [EPR35] to describe an equivalent protocol and prove that its security is inherent in the laws of quantum mechanics. That is, so long as the quantum theory is not shown to be incomplete the protocol will remain absolutely secure [Eke91]. The BB84 protocol has become

widely known in recent years, however it was not generally looked upon as more than an academic exercise until a *Scientific American* article published by Bennet, Brassard, and Ekert not only popularized the idea of 'quantum cryptography' but showed the world that it could be performed in a laboratory environment [BBE92]. Despite being commonly called quantum cryptography, a more accurate description is given by the term 'quantum key distribution' (QKD), since quantum mechanics plays a role only in distributing a key between two parties. Once they are in possession of the key, any cryptography performed with it is classical in nature.

QKD has come a long way since 1984. It is now possible to purchase commercial, off-the-shelf systems that will provide point-to-point, unconditionally secure channels over standard telecommunication optical fibres. Such systems include a range of offerings from id Quantique in Geneva as well as MagiQ Technologies in New York. Of particular interest to experimental research groups working with any aspect of QKD is the id Quantique Clavis Plug&Play system [id 05], which is designed to be both versatile and stable while allowing custom control via user-created C++ programs and integration with other optical components. However, despite all of this progress there is still a basic limitation to all current QKD implementations. Losses within optical fibres, or even free space, increase with the distance between two communicating parties. There is a fundamental limit above which the noise-to-signal ratio, known as the 'quantum bit error rate', becomes so large that no secret key can be distributed. Furthermore, the rate at which the key can be generated drops dramatically as this distance limit is approached. Current implementations such as the Plug&Play system state limits on the order of 100 km.

1.1.1 The BB84 protocol

There are many extant descriptions of the BB84 protocol and its derivatives. Those of a pedagogical nature include the textbooks by Nielsen and Chuang [NC00] and by Le Bellac

[LB06]. This is not the place for another in-depth discussion of the protocol, yet some parts of this work are strongly motivated by aspects of its experimental implementation. Therefore it will be useful to provide a summary of the key points that allow BB84 to provide unconditional security. For simplicity it will be assumed that detectors and transmission lines are perfect.

In discussions of cryptographic protocols is is common to give names to the parties involved, typically assigned alphabetically. Following the common standard, consider a scenario in which Alice and Bob wish to generate a secret key without meeting, and with certainty that the notorious eavesdropper Eve gains no information from them. In order to do so, Alice sends to Bob a photon that is linearly polarized along one of four axes, aligned at 0 (horizontal), $\pi/2$ (vertical), and $\pm\pi/4$ ($\pm$diagonal) with respect to the horizontal axis. Her choice of axis is random, and when Bob receives the photon he measures its polarization in either the horizontal-vertical basis or the $\pm$diagonal basis, also chosen randomly. He then publicly announces to Alice which basis he chose, but not the result of his measurement. If she chose an axis from the same basis then she knows with certainty his measurement result, and they share a key bit. If the photon was originally prepared along one of the other two axes, she tells Bob to discard his result. This process repeats until Alice and Bob share enough key bits to safely encrypt their message. In order to determine whether Eve attempted to listen, Alice and Bob publicly declare the values of a subset of their key bits. If they all match, then Alice and Bob can be confident that their remaining secret bits also match. Figure 1.1 contains a reproduction of the hypothetical run of the protocol as originally presented in Bangalore by Bennett and Brassard.

1.1.2 Extending the range of QKD

As already mentioned, existing QKD implementations have a finite range, due to the fact that no method of transmission can be truly lossless, and since the losses increase with distance while the level of detector noise remains constant, the signal-to-noise ratio approaches zero. This problem is circumvented in classical telecommunications by the use of repeaters – devices which read a signal before it has degraded to uselessness, then amplify and re-transmit it. By chaining such repeaters together, there is no limit to the distance over which classical communications can occur. Unfortunately in the case of quantum information, the same property that guarantees security also prevents the use of traditional repeaters; any attempt to read the information in order to amplify it will instead destroy the quantum nature of the state. However, there are proposals for other methods to solve this problem. The simplest theoretical solution is to have a *trusted* site every 100 km or so along the desired transmission path. Each of these sites can then create a secret key with its neighbours, and ultimately pass the message the entire length of the chain. In practice of course, it is dangerous to assume that such a sequence of sites will exist, and impractical on a large scale to hope that all possible pairs of people who wish to communicate across a network will trust every node in the network.

QUANTUM TRANSMISSION															
Alice's random bits.....	0	1	1	0	1	1	0	0	1	0	1	1	0	0	1
Random sending bases.....	D	R	D	R	R	R	R	R	D	D	R	D	D	D	R
Photons Alice sends.....	↗	↕	↘	↔	↕	↕	↔	↔	↘	↗	↕	↘	↗	↗	↕
Random receiving bases.....	R	D	D	R	R	D	D	R	D	R	D	D	D	D	R
Bits as received by Bob.....	1		1		1	0	0	0		1	1	1		0	1
PUBLIC DISCUSSION															
Bob reports bases of received bits.....	R		D		R	D	D	R		R	D	D		D	R
Alice says which bases were correct.....			OK		OK			OK				OK		OK	OK
Presumably shared information (if no eavesdrop)...			1		1			0				1		0	1
Bob reveals some key bits at random.....					1									0	
Alice confirms them.....					OK									OK	
OUTCOME															
Remaining shared secret bits.....			1					0				1			1

Figure 1.1: The original example of the BB84 protocol, reproduced from the paper of Bennett and Brassard [BB84]. The bases are labeled 'R' for rectilinear, corresponding to the axes at 0 and $\pi/2$; and 'D' for diagonal, those at $\pm\pi/4$.

A more promising method that allows arbitrary extension of the distance over which keys can be generated, without requiring any additional trusted sites, makes use of so-called quantum repeaters [BDCZ98, DLCZ01]. As with quantum cryptography, the term 'quantum repeater' is something of a misnomer; the proposal is however to provide a method of obtaining the result that a repeater would offer, if the quantum no-cloning theorem didn't forbid it [WZ82]. What the protocol actually allows for is also known as entanglement swapping, which better describes the physical mechanism behind its achievement. Briefly, the protocol functions as follows. Two parties who wish to communicate securely but are too far apart to implement QKD each generate a pair of maximally-entangled photons, keeping one half of the pair and sending the other half to a centrally-located third party. When both photons have arrived, a Bell-state measurement is performed on them. This results in the other halves of the original photon pairs becoming entangled, which in turn allows a QKD protocol to be enacted. Obviously under this description the maximum distance over with QKD can be implemented is merely doubled, but the process can be easily chained together as many times as necessary to cover an arbitrary distance. It is worth noting that the two communicators do not need to trust the third party (or parties, in the case of multiple steps between them) in order for the protocol to work.

The integral component that allows the entanglement-swapping protocol to work efficiently over large distances is a method by which a photon can be 'paused' at a certain location. This then allows the two communicators to each store a photon while waiting for the protocol to complete. There is also the possibility that either of the photons might not arrive at the central location, due to losses in the transmission medium. The probability of successfully implementing the protocol increases when it is possible to store one photon until the other has arrived. As may be evident by now, the role of photons in quantum information in general, and in QKD specifically, is to be information carriers.

This pausing of the photon is therefore seen as analogous to storing or 'remembering' the photon's information, so devices capable of performing this task are generally referred to as 'quantum memories'.

1.2 Quantum memory

The goal of any quantum memory for photons is to keep in one place, for a specified period of time, the information encoded in a quantum state of light. After the desired time has passed, the information should then continue to propagate at the speed of light. One method for achieving this goal is to radically slow or even stop the light by affecting the refractive index of a medium. Achieving this is generally based on the idea of electromagnetically-induced transparency (EIT) [HFI90, BIH91]. The phenomenon of EIT allows an otherwise-opaque medium to be rendered transparent to a given probe pulse by use of a strong control field. If the control field is switched off while the probe is still inside the medium, the pulse cannot continue propagating effectively, and so remains trapped within the medium until the control is switched back on. This was first achieved by Hau *et al.* in 1999 when they slowed light to 17 m/s [HHDB99]. A year later it was proposed to make use of this method as a quantum memory [FL00], and experimental storage of classical light fields in trapped Sodium [LDBH01] and in atomic Rubidium vapour [PFM$^+$01] soon followed. Storage of quantum states of light has also been achieved more recently by various groups [AEW$^+$05, CMJ$^+$05, AFK$^+$08].

Another common method for attempting to store quantum states of light is to coherently transfer, in a reversible manner, the relevant quantum information from the state of the light to the state of either a single trapped atom or a solid-state ensemble of many atoms. The case of interactions between a photon and a single trapped atom is the domain of cavity quantum electrodynamics; Jeff Kimble's group has proposed and begun

experimental investigations into such a memory [BBM+07]. When many more atoms are involved, the system can be treated as a statistical ensemble. It is in this regime that protocols based on controlled reversible inhomogeneous broadening of the medium's absorption profile (CRIB) can be employed, and it is this basis for quantum state storage which the current work explores and to which it adds. As it is the foundation for the current work, a detailed description of the CRIB protocol is left until Chapter 3, wherein a detailed analysis is presented, following the work of Sangouard *et al.* [SSAG07], while including calculations in a more general, non-ideal setting.

1.3 Manipulating qubits

Fundamental not only to QKD but to any quantum information processing application is the ability to manipulate qubits. When the qubits are encoded in photons, this obviously entails an optical setup of some sort. It has been shown that an arbitrary optical setup can always be decomposed into a combination of beam splitters and phase shifters [RZBB94], which can therefore be thought of as fundamental units or building blocks for manipulating photonic states. For example, in the BB84 protocol it is necessary to be able to prepare a set of four appropriate states, and perform projection measurements onto each of them. The most intuitive of these sets of states is generally held to be that described in Section 1.1.1, based on polarization. This choice is not well adapted for communications over standard optical fibres though, as fibres may not preserve the state of polarization of transmitted light. A more common approach is to make use of time windows, or bins, to define qubits. Instead of associating the bit values 0 and 1 with horizontal and vertical polarization respectively, as done in Figure 1.1, the bits 0 and 1 can be assigned to photons arriving in the first (early) or second (late) time bin, for example [BGTZ99]. This then implies that the analogue of the $\pm\pi/4$ polarization states must be

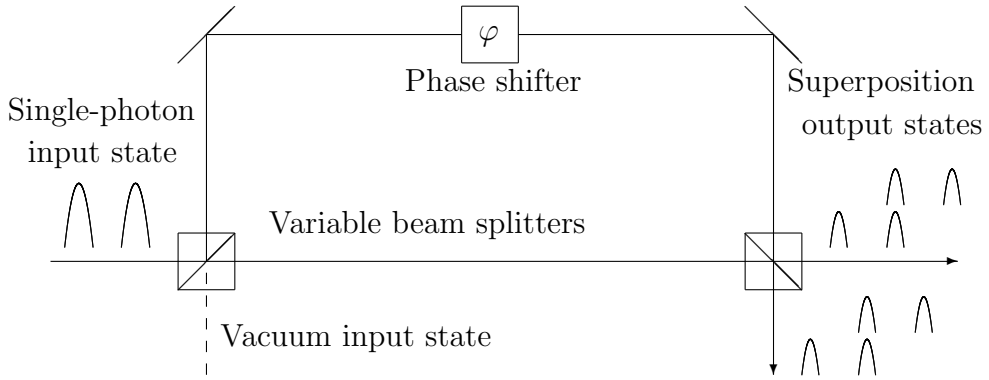

Figure 1.2: A schematic representation of the traditional method of making a measurement in a time-bin basis. A photon in an arbitrary superposition of two time bins is sent into the first beam splitter. If the path-length difference between the two arms corresponds to the time delay between the two time bins, there will be three bins to consider at each output.

given by a photon in a superposition of being early and late. In general the creation and measurement of such a state is achieved by use of an interferometer, as shown in Figure 1.2, which is composed of two beam splitters and a phase shifter. This method works well for creating the states, and also works perfectly, in theory, for making measurements. It also works well in practice, however, in order for Alice and Bob to obtain useful results they must each have an interferometer, and the path-length differences of the pair must be stabilized to within a small fraction of the photon's wavelength over distances of up to 100 km. The need for this stabilization arises due to the fact that Alice and Bob must use the same definition of $|\text{early}\rangle$ and $|\text{late}\rangle$ in order for the protocol to work. This can already be achieved experimentally, although a method that removed the need for long-distance stabilization and which made use of a device with other applications in QKD would have distinct advantages. Another method of manipulating states, known as Raman adiabatic transfer of optical states (RATOS), has been proposed in the context of EIT [AML06]. The RATOS scheme makes use of multiple optical control fields and an ensemble of atoms that possess an energy level structure containing a so-called multi-Λ configuration in order to transfer photons between two optical modes.

In Chapter 4 a new method for performing the same tasks as beam splitters and phase shifters is presented. It also makes use of atomic ensembles, although being based on a modification of the CRIB protocol means that it requires only a two-level system. This new method allows the same physical device to be employed as a quantum memory, a beam splitter, and a phase shifter. It requires only the ability to control classical static electric fields, so has the potential to be experimentally simpler than the interferometer-based methods currently in use. Furthermore, the method is also able to prepare the requisite BB84 states.

1.4 Document structure

In Chapter 2 the background theory required for a discussion of the CRIB protocol is reviewed. This consists primarily of the Maxwell-Bloch equations, and is where many notations and concepts are introduced. As already mentioned, Chapters 3 and 4 provide a detailed investigation of the CRIB protocol in a non-ideal medium, and the proposed modifications to it that allow arbitrary time-bin qubits to be created and the tasks of a beam splitter and phase shifter to be replicated in the storage device. With the new protocol well-defined, Chapter 5 presents the method used in this work to simulate the evolution of the modified system, along with various results from the simulations and their interpretations. Finally some concluding remarks can be found in Chapter 6. The code that was used to create the simulation results is presented in Appendix A, and a summary of symbols and notation can be found in Appendix B.

Chapter 2

Background

2.1 Theoretical framework

A description of the CRIB protocol relies on a description of the interaction of a weak electric field with an ensemble of absorbers. Thus before investigating the protocol in detail, a theoretical framework able to describe such an interaction must be established. The appropriate theory is contained in the Maxwell-Bloch equations, which describe the interaction of a classical light field and an ensemble of quantized two-level atoms. In the present case the light field is assumed to be a pulse of finite temporal width. This pulse is likely to come from a laser so it is well justified to consider a one-dimensional electric field of the form

$$\mathbf{E}_{\mathrm{f}}(z,t) = \boldsymbol{\varepsilon}\mathcal{E}_{\mathrm{f}}(z,t)\mathrm{e}^{-\mathrm{i}(\omega_L t - kz)} + \mathrm{c.c.}\ , \tag{2.1}$$

where $\mathcal{E}_{\mathrm{f}}$ is a function describing the pulse envelope, and is assumed to be real. Here the subscript 'f' refers to a forward-propagating pulse, i.e. one moving in the positive z direction; later 'b' subscripts will be introduced for a backward-moving pulse.

The state of a single two-level atom can be described by a density operator $\hat{\rho}(t)$ that evolves according to the Schrödinger equation. This leads to the definition of the Bloch vector, $\mathbf{r}(t) = \sum_{i=1}^{3} r_i(t)\hat{\mathbf{e}}_i$, specified by the three components

$$r_1 = 2\mathrm{Re}(\rho_{12})\ , \tag{2.2a}$$

$$r_2 = 2\mathrm{Im}(\rho_{12})\ , \tag{2.2b}$$

$$r_3 = \rho_{22} - \rho_{11}\ . \tag{2.2c}$$

The chosen basis in which to work is that of the atomic Hamiltonian, $\hat{H}_A$, with $|1\rangle$ and $|2\rangle$

representing the ground state and excited state, respectively. For example $\rho_{12} = \langle 1|\hat{\rho}|2\rangle$. Such an atom will have a resonance frequency ω_0, from which the laser is detuned by an amount Δ. That is, for $i \in \{1, 2\}$, $\hat{H}_A|i\rangle = \hbar\omega_i|i\rangle$ and

$$\omega_2 - \omega_1 =: \omega_0 = \omega_L + \Delta \ . \tag{2.3}$$

The absorption profile of the medium as a whole is equivalent to a distribution of spectral components within the medium, given by a function $g(\Delta)$ satisfying

$$\int_{-\infty}^{\infty} \mathrm{d}\Delta \, g(\Delta) = 1 \ ; \tag{2.4}$$

that is, 100% of the atoms must have *some* detuning. Each atom has some natural linewidth centred on its resonance frequency. This width, assumed to be the same for all the atoms in the medium, is known as the 'homogeneous linewidth' and denoted Γ_{h}. However, in any solid medium there are localized stresses and strains which modify the energy levels of individual atoms, resulting in different resonance frequencies for different absorbers. In particular this is true in the case of rare-earth-ion-doped crystals and locally crystalline media, such as optical fibres. The stresses and strains create a spatially inhomogeneous potential, resulting in variations of the resonant frequencies present in the ensemble. The net result of this is an absorption profile for the medium that is wider than the profile of any individual absorber within it; the width of this profile is the 'inhomogeneous linewidth' and is denoted Γ_{ih}. In addition, external factors such as electric or magnetic fields may further broaden the range of transition frequencies present within the sample. This results in a cumulative absorption profile that is significantly wider than the individual profile of any given absorber. This profile in frequency space, relative to the laser frequency ω_L, is the detuning profile $g(\Delta)$.

If the medium as a whole is now considered to be comprised of a continuum of two-level atoms, with a corresponding Bloch vector at each position z and for each detuning Δ, distributed according to $g(\Delta)$, then the state of the medium can be described by

a continuous field of Bloch vectors, $\mathbf{r}(z,t,\Delta)$. With this description of the medium its polarization $\mathbf{P}(z,t)$, appearing in Maxwell's equations, is given by

$$\mathbf{P}(z,t) = \frac{N}{2}\int_{-\infty}^{\infty} \mathrm{d}\Delta\, g(\Delta)\boldsymbol{\mu}_{12}\left[r_1(z,t,\Delta) - \mathrm{i}r_2(z,t,\Delta)\right] + \text{c.c.} \tag{2.5}$$

where N is the density of atomic dipoles in the medium, and the atomic dipole moment $\boldsymbol{\mu}_{12} = \langle 1|\hat{\boldsymbol{\mu}}|2\rangle$ is the off-diagonal element of the dipole operator $\hat{\boldsymbol{\mu}}$. This expression suggests a definition which will prove to be convenient, that of the atomic polarization

$$\sigma(z,t,\Delta) := r_1(z,t,\Delta) - \mathrm{i}r_2(z,t,\Delta)\ . \tag{2.6}$$

As the light propagates within the medium it induces a wave of polarization whose phase will match that of the electric field. It is therefore useful to further define slowly-varying forward- and backward-moving components of the polarization via

$$\sigma(z,t,\Delta) =: \sigma_{\mathrm{f}}(z,t,\Delta)\mathrm{e}^{-\mathrm{i}(\omega_L t - kz)} + \sigma_{\mathrm{b}}(z,t,\Delta)\mathrm{e}^{-\mathrm{i}(\omega_L t + kz)}\ . \tag{2.7}$$

Of course, so long as there has only been a pulse moving in the forward direction σ_{b} will vanish.

2.2 The Bloch equations

The goal of this chapter is to derive a set of equations that govern the evolution of a light pulse (or more specifically its envelope function) within a solid-state medium, and of the medium itself. These will be the well-known Maxwell-Bloch equations [MW95]. The first step will be to derive the evolution of the atomic polarization in the presence of an external electric field. To begin, consider the behaviour of the Bloch vector under the influence of an interaction Hamiltonian $\hat{H}_I$. The equations of motion for $\mathbf{r}$ are straightforward to derive from Schrödinger's equation; they are the Bloch equations [Blo46], a

set of coupled differential equations,

$$\partial_t r_1 = \frac{2}{\hbar}\mathrm{Im}\left(\langle 1|\hat{H}_I|2\rangle\right) r_3 - \omega_0 r_2 \ , \tag{2.8a}$$

$$\partial_t r_2 = -\frac{2}{\hbar}\mathrm{Re}\left(\langle 1|\hat{H}_I|2\rangle\right) r_3 + \omega_0 r_1 \ , \tag{2.8b}$$

$$\partial_t r_3 = -\frac{2}{\hbar}\mathrm{Im}\left(\langle 1|\hat{H}_I|2\rangle\right) r_1 + \frac{2}{\hbar}\mathrm{Re}\left(\langle 1|\hat{H}_I|2\rangle\right) r_2 \ . \tag{2.8c}$$

The case of interest here involves the interaction between the light field and the atomic dipoles in the medium, and it is assumed that the light is propagating in the forward direction. The interaction Hamiltonian, $\hat{H}_I$, is thus of the well-known form

$$\hat{H}_I = -\hat{\boldsymbol{\mu}} \cdot \mathbf{E}_\mathrm{f} \ . \tag{2.9}$$

The result of the inner product in (2.9) depends on the nature of the atomic transition and on the polarization of the light field. It is generally assumed that the atomic transition of the medium is known and that the polarization state of the light can be chosen to maximize the probability of the transition occuring. That is, linearly-polarized light will be chosen for the case of an atomic $\Delta m = 0$ transition, while circularly-polarized light will be selected given a $\Delta m = \pm 1$ transition. These two cases result in different equations of motion for the Bloch vector, but under the rotating wave approximation they become equivalent [MW95]. This approximation consists of neglecting rapidly-oscillating components which vanish on average over any appreciable time scale. The resulting equations are,

$$\partial_t r_1 = -\frac{2\wp\mathcal{E}_\mathrm{f}}{\hbar}\sin(\omega_L t - kz) r_3 - \omega_0 r_2 \ , \tag{2.10a}$$

$$\partial_t r_2 = \frac{2\wp\mathcal{E}_\mathrm{f}}{\hbar}\cos(\omega_L t - kz) r_3 + \omega_0 r_1 \ , \tag{2.10b}$$

$$\partial_t r_3 = \frac{2\wp\mathcal{E}_\mathrm{f}}{\hbar}\sin(\omega_L t - kz) r_1 - \frac{2\wp\mathcal{E}_\mathrm{f}}{\hbar}\cos(\omega_L t - kz) r_2 \ , \tag{2.10c}$$

where

$$\wp := \boldsymbol{\mu}_{12} \cdot \boldsymbol{\varepsilon}^* \tag{2.11}$$

can be assumed to be real based on an appropriate choice of light polarization for the type of atomic transition.

There is a final simplifying step that can be made, that of switching into the so-called rotating frame. This is achieved by noting that most of the terms in these equations of motion oscillate with frequency $\omega_L t - kz$, and therefore choosing to define a pair of new components r'_1 and r'_2 via

$$r'_1 - \mathrm{i}r'_2 := (r_1 - \mathrm{i}r_2)\,\mathrm{e}^{\mathrm{i}(\omega_L t - kz)} \ . \tag{2.12}$$

Note that this definition is equivalent to those anticipated by (2.6) and (2.7) for the case in which there is no backward-moving polarization wave, $\sigma_\mathrm{b} = 0$, namely

$$\sigma_\mathrm{f} = \sigma \mathrm{e}^{\mathrm{i}(\omega_L t - kz)} \ . \tag{2.13}$$

Furthermore, the definition of $\mathbf{r}'$, the Bloch vector in the rotating frame, is completed by setting $r'_3 := r_3$. The equations of motion for the components of this vector are then given by

$$\partial_t r'_1 = \Delta r'_2 \ , \tag{2.14a}$$

$$\partial_t r'_2 = -\Delta r'_1 + \frac{2\wp \mathcal{E}_\mathrm{f}}{\hbar} r'_3 \ , \tag{2.14b}$$

$$\partial_t r'_3 = -\frac{2\wp \mathcal{E}_\mathrm{f}}{\hbar} r'_2 \ . \tag{2.14c}$$

From (2.12) and (2.13) it is clear that $\sigma_\mathrm{f} = r'_1 - \mathrm{i}r'_2$; from this and (2.14) the equation of motion for σ_f is found to be

$$\partial_t \sigma_\mathrm{f}(z,t,\Delta) = \mathrm{i}\Delta\sigma_\mathrm{f}(z,t,\Delta) - \mathrm{i}\frac{2\wp}{\hbar}\mathcal{E}_\mathrm{f}(z,t) r_3(z,t,\Delta) \ . \tag{2.15}$$

In the low-excitation limit, eminently valid for the case of a large number of atoms interacting with a weak field equivalent to a small number of photons, the vast majority of the atoms remain unexcited. As can be seen from (2.2c) this means that $r_3 \approx -1$.

Under this assumption the equation of motion for the polarization becomes

$$\partial_t \sigma_{\mathrm{f}}(z,t,\Delta) = \mathrm{i}\Delta\sigma_{\mathrm{f}}(z,t,\Delta) + \mathrm{i}\frac{2\wp}{\hbar}\mathcal{E}_{\mathrm{f}}(z,t) \ . \tag{2.16a}$$

When the only electric field present in the medium is a backward-propagating pulse, similar considerations result in the same equation of motion for the corresponding polarization wave,

$$\partial_t \sigma_{\mathrm{b}}(z,t,\Delta) = \mathrm{i}\Delta\sigma_{\mathrm{b}}(z,t,\Delta) + \mathrm{i}\frac{2\wp}{\hbar}\mathcal{E}_{\mathrm{b}}(z,t) \ . \tag{2.16b}$$

These two equations describe the behaviour of the ensemble of dipoles in the medium in the presence of an electric field. The next step will be to determine the behaviour of the electric field in the presence of this atomic polarization.

2.3 Maxwell-Bloch equations

A good starting point when examining the behaviour of an electromagnetic field is always provided by Maxwell's equations. They yield the wave equation for light in a polarized medium,

$$\left(\partial_z^2 - \frac{n^2}{c^2}\partial_t^2\right)\mathbf{E}_{\mathrm{f}}(z,t) = \frac{1}{\epsilon_0 c^2}\partial_t^2 \mathbf{P}(z,t) \ . \tag{2.17}$$

Here n denotes the refractive index of a transparent background medium in which the medium with polarization $\mathbf{P}$ is embedded. In particular this may represent a polarizable ensemble of rare-earth ions doped into a glass or crystal. The polarization can be expressed in terms of the collective state of the atomic dipoles using (2.5). Along with the slowly-varying envelope approximations

$$\left|\partial_t^2 \mathcal{E}_{\mathrm{f}}\right| \ll \omega_L \left|\partial_t \mathcal{E}_{\mathrm{f}}\right| \ll \omega_L^2 \left|\mathcal{E}_{\mathrm{f}}\right| \quad \text{and} \quad \left|\partial_z^2 \mathcal{E}_{\mathrm{f}}\right| \ll k \left|\partial_z \mathcal{E}_{\mathrm{f}}\right| \ll k^2 \left|\mathcal{E}_{\mathrm{f}}\right| \tag{2.18}$$

this results in the paraxial wave equation

$$\left(\frac{n}{c}\partial_t + \partial_z\right)\mathcal{E}_{\mathrm{f}}(z,t) = \mathrm{i}\frac{\omega_L N \wp}{4\epsilon_0 n c}\int_{-\infty}^{\infty} \mathrm{d}\Delta \, g(\Delta)\sigma_{\mathrm{f}}(z,t,\Delta) \ . \tag{2.19a}$$

Under the same conditions the backward-moving field is governed by

$$\left(\frac{n}{c}\partial_t - \partial_z\right)\mathcal{E}_{\mathrm{b}}(z,t) = \mathrm{i}\frac{\omega_L N \wp}{4\epsilon_0 n c}\int_{-\infty}^{\infty}\mathrm{d}\Delta\, g(\Delta)\sigma_{\mathrm{b}}(z,t,\Delta)\ . \tag{2.19b}$$

At this point there are two possibile paths forward. The first results in the full, general form of the Maxwell-Bloch equations: from the definition of σ_{f}, (2.19a) is equivalent to

$$\left(\frac{n}{c}\partial_t + \partial_z\right)\mathcal{E}_{\mathrm{f}}(z,t) = \mathrm{i}\frac{\omega_L N \wp}{4\epsilon_0 n c}\int_{-\infty}^{\infty}\mathrm{d}\Delta\, g(\Delta)\left[r_1'(z,t,\Delta) - \mathrm{i}r_2'(z,t,\Delta)\right] \tag{2.20}$$

which, on comparison of real and imaginary parts, simplifies to

$$\left(\frac{n}{c}\partial_t + \partial_z\right)\mathcal{E}_{\mathrm{f}}(z,t) = \frac{\omega_L N \wp}{4\epsilon_0 n c}\int_{-\infty}^{\infty}\mathrm{d}\Delta\, g(\Delta) r_2'(z,t,\Delta)\ . \tag{2.21}$$

The combination of (2.21) and the evolution of r_2' as governed by (2.14) yields the Maxwell-Bloch equations (a similar result holds for the backward-moving components).

On the other hand, one can make use of (2.16) to evolve the atomic polarization in the low-excitation limit, in which case the light field is governed by (2.19). These coupled differential equations provide a simplified form of the Maxwell-Bloch equations that is particularly useful for describing the CRIB protocol for quantum memory.

In order to further simplify the notation used it is common to define the Rabi frequency

$$\Omega(z,t) := \frac{2\wp}{\hbar}\mathcal{E}(z,t) \tag{2.22}$$

and to define a constant

$$\beta := \frac{\omega_L N \wp^2}{2\epsilon_0 \hbar n c}\ . \tag{2.23}$$

The Maxwell-Bloch equations are presented using these conventions in the next chapter, along with a detailed description and analysis of the CRIB protocol. While Ω has units of Hz, it differs from the electric field only by a constant factor. For this reason one may refer to Ω as the light field, and in fact this is done frequently in the subsequent chapters.

Chapter 3

The CRIB protocol

The CRIB protocol for quantum memory describes a method by which a given state of light can be stored in the coherences of an ensemble of atomic dipoles embedded in an otherwise-transparent solid. The process is similar to that of photon echoes [KAH64, AKH66]; light is absorbed coherently by the ensemble, the members of which begin to dephase with respect to one another. A hidden time-reversal symmetry of the system is then exploited to cause the atoms to begin rephasing, so that a time-reversed copy of the input light is re-emitted, propagating in the opposite direction [MK01, NK05, KTG$^+$06, SSAG07]. Modifications to the original protocol that allow for high-efficiency recall in the forward direction have also been propsed, and initial experimental tests have yielded recall efficiencies of up to 15% [ALSM06, HLA$^+$08].

A detailed description of the CRIB protocol is the subject of the following sections, but it is instructive to begin with an outline of its general form. A light pulse to be stored travels forward in the positive z direction through a transparent medium toward the storage medium, which contains an ensemble of atomic dipoles. These absorbers exist for $z \in [0, L]$, where L is the length of the medium. Inside the medium some portion of the pulse gets absorbed; ideally absorption is complete, but for finite optical depth some percentage of the pulse will exit the medium at $z = L$ and be lost from the system. Some time after the absorption it is possible to perform some action that results in the recall of the pulse, which exits the medium at $z = 0$ propagating backward, in the negative z direction.

3.1 Finding time-reversal symmetry

The coupled equations of motion for a light field propagating in a polarizable medium and that medium's polarization were seen at the end of Chapter 2; they are restated here for convenience. The forward-moving components evolve under

$$\left(\frac{n}{c}\partial_t + \partial_z\right)\Omega_{\mathrm{f}}(z,t) = \mathrm{i}\beta\int_{-\infty}^{\infty}\mathrm{d}\Delta\, g(\Delta)\sigma_{\mathrm{f}}(z,t,\Delta)\ , \tag{3.1a}$$

$$\partial_t\sigma_{\mathrm{f}}(z,t,\Delta) = \mathrm{i}\Delta\sigma_{\mathrm{f}}(z,t,\Delta) + \mathrm{i}\Omega_{\mathrm{f}}(z,t)\ , \tag{3.1b}$$

while the backward-moving components obey

$$\left(\frac{n}{c}\partial_t - \partial_z\right)\Omega_{\mathrm{b}}(z,t) = \mathrm{i}\beta\int_{-\infty}^{\infty}\mathrm{d}\Delta\, g(\Delta)\sigma_{\mathrm{b}}(z,t,\Delta)\ , \tag{3.2a}$$

$$\partial_t\sigma_{\mathrm{b}}(z,t,\Delta) = \mathrm{i}\Delta\sigma_{\mathrm{b}}(z,t,\Delta) + \mathrm{i}\Omega_{\mathrm{b}}(z,t)\ . \tag{3.2b}$$

The essence of CRIB lies in a hidden time reversal symmetry of these equations, which becomes apparent under the correct circumstances. To find the symmetry, first recall that $g(\Delta)$ describes the distribution of detunings within the medium, i.e. how the transition frequencies within the ensemble of dipoles are distributed around the central frequency ω_L. Now suppose that at some time T_0, after the light pulse described by $\mathcal{E}_{\mathrm{f}}$ has been absorbed by the medium, it is possible to mirror the detuning distribution about its centre, setting $g(\Delta) \to g(-\Delta)$. The polarization of an atom that was initially detuned by Δ will remain unchanged when the atom's detuning is switched to $-\Delta$, resulting in $\sigma(z,t,\Delta) \to \sigma(z,t,-\Delta)$. Under the assumption that there is no electric field within the medium at time T_0, a π phase shift is automatically applied to the field since $\Omega_{\mathrm{f}}(z,T_0) = 0 = -\Omega_{\mathrm{f}}(z,T_0)$ for each z inside the medium. Substituting these transformed quantities into (3.1) shows that the equations transform to

$$\left(\frac{n}{c}(-\partial_t) - \partial_z\right)\Omega_{\mathrm{f}}(z,t) = \mathrm{i}\beta\int_{-\infty}^{\infty}\mathrm{d}\Delta\, g(\Delta)\sigma_{\mathrm{f}}(z,t,\Delta)\ , \tag{3.3a}$$

$$-\partial_t\sigma_{\mathrm{f}}(z,t,\Delta) = \mathrm{i}\Delta\sigma_{\mathrm{f}}(z,t,\Delta) + \mathrm{i}\Omega_{\mathrm{f}}(z,t)\ . \tag{3.3b}$$

It is now clear that under time reversal, $t \to -t$, these equations become

$$\left(\frac{n}{c}\partial_t - \partial_z\right)\Omega_{\rm f}(z,-t) = {\rm i}\beta\int_{-\infty}^{\infty}{\rm d}\Delta\, g(\Delta)\sigma_{\rm f}(z,-t,\Delta)\ , \tag{3.4a}$$

$$\partial_t\sigma_{\rm f}(z,-t,\Delta) = {\rm i}\Delta\sigma_{\rm f}(z,-t,\Delta) + {\rm i}\Omega_{\rm f}(z,-t)\ . \tag{3.4b}$$

On comparison with (3.2) it can be seen by making the identifications

$$\Omega_{\rm b}(z,t) = \Omega_{\rm f}(z,-t) \quad \text{and} \quad \sigma_{\rm b}(z,t,\Delta) = \sigma_{\rm f}(z,-t,\Delta) \tag{3.5}$$

that the equations of motion for a forward-moving pulse have been transformed into those for a time-reversed copy of the same pulse propagating in the backward direction. That is, light that has been absorbed while propagating in the forward direction can be recalled from the medium after some delay; the field will be re-emitted propagating in the backward direction. This means that the system can be used as a memory for storing the light if a method can be found for causing the equations of motion for the system to switch from (3.1) to (3.2). There are indeed methods for doing just that, and they will be investigated in the next sections.

Before proceeding though one further requirement for triggering the recall of the pulse must be noted; there is a subtlety in making the assignment $\sigma_{\rm b}(z,t,\Delta) = \sigma_{\rm f}(z,-t,\Delta)$. Recall the definition (2.7) of the components of the atomic polarization in the medium:

$$\sigma(z,t,\Delta) = \sigma_{\rm f}(z,t,\Delta){\rm e}^{-{\rm i}(\omega_L t - kz)} + \sigma_{\rm b}(z,t,\Delta){\rm e}^{-{\rm i}(\omega_L t + kz)}\ . \tag{3.6}$$

It is clear that $\sigma_{\rm f}$ is the component propagating in the $+z$ direction, so in order for the system to evolve backward a $2kz$ phase shift must be applied to the medium such that

$$\sigma_{\rm b}(z,t,\Delta){\rm e}^{-{\rm i}(\omega_L t + kz)} = {\rm e}^{-2ikz}\sigma_{\rm f}(z,-t,\Delta){\rm e}^{-i(\omega_L t - kz)} = \sigma_{\rm f}(z,-t,\Delta){\rm e}^{-i(\omega_L t + kz)}\ . \tag{3.7}$$

Without this phase shift the polarization wave within the medium, and therefore the recalled pulse, will continue to propagate in the forward direction, and the time-reversal symmetry will be lost.

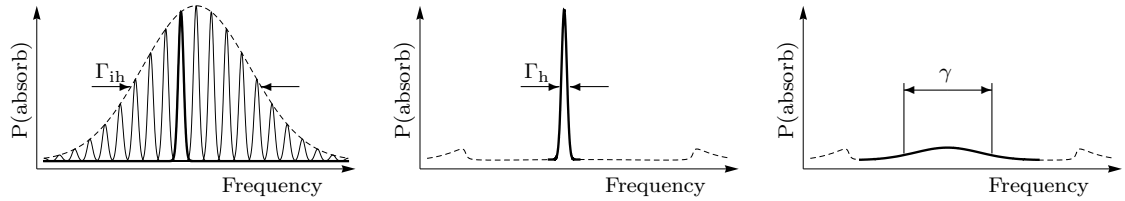

(a) Naturally broadened profile of inhomogeneous linewidth Γ_{ih}

(b) Anti-hole burning results in the homogeneous linewidth Γ_h

(c) Artificially, reversibly broadened profile of width γ

Figure 3.1: Probability for light to be absorbed in the medium as a function of frequency during the preparatory stages of the CRIB protocol. (a) Initially each dipole in the storage medium has a narrow homogeneous linewidth. The probability for the medium to absorb a photon at a given frequency depends on the number of dipoles at that frequency (solid lines); collectively this range of resonance frequencies provides a much wider inhomogeneous absorption spectrum (dashed line). For clarity an arbitrary homogeneous line has been picked out (bold line). (b) After employing spectral hole burning techniques only a single absorption peak remains, within a certain frequency window. (c) An external electric field gradient is applied to the medium, causing a broadening of the absorption peak. The total area under the absorption line remains constant as it widens.

3.2 Implementation

The results of the previous section show that a memory based on complete time-reversal of the input light field can be achieved in a system for which the absorption spectrum can be controllably reversed, $g(\Delta) \rightarrow g(-\Delta)$. Of course, the linewidth must also be broad enough to absorb all Fourier components of the incoming pulse. This can obviously not be achieved with every possible choice for the polarizable medium. In fact there currently is no definitive choice as to which material provides the best possibility for CRIB. Even as investigations continue it is unlikely that a single medium will become ubiquitous, since the choice will still depend on parameters such as the frequency of light to be stored and the required storage duration. There is agreement that locally crystalline structures doped with a low concentration of rare-earth ions provide all of the necessary properties, yet determining what rare-earth element should be added to which medium is still an active area of research. One potential candidate is Erbium-doped optical fibres [HSSA$^+$06, Sta08], which are already used extensively in classical telecommunication.

Two well-studied rare-earth elements are Europium and Praseodymium, generally doped into crystals such as Y_2SiO_5 [Ale07]. The properties of Thulium as the dopant are also being investigated, in YAG and Y_2O_3 [Cha08], as well as Erbium-doped Y_2SiO_5, Y_2O_3, $LiNbO_3$, YAG, $YAlO_3$, $CaWO_4$, and $SrWO_4$ [STC$^+$02], and Er^{3+}:$LiNbO_3$ along with Neodymium-doped YVO_4 and Y_2SiO_5[Sta08].

Because of this wide range of choices, all of which are in the relatively early stages of investigation, there do not exist 'typical' values for many of the parameters involved. For example, optical coherence times can range from nanoseconds to milliseconds for different ions. For the purposes of the current discussion, when numerical values are required they will be taken from the investigation of Erbium as a dopant, performed by Staudt [Sta08]. With that in mind, each ion in the ensemble can have a relatively narrow homogeneous linewidth as depicted in Figure 3.1, on the order of 50 Hz to a few kHz. However, stresses and strains within the local crystalline structure have the effect of shifting the central frequencies of these lines. This results in the medium containing a spectrum of classes of narrow absorption lines which combine to create a much broader line width ($\sim$1 GHz). This can be seen graphically in Figure 3.1(a).

The overall natural spectrum of the medium is wide, as required, however it cannot be reversed about its central frequency. Therefore further preparation of the medium is needed. A single narrow peak can be obtained via spectral hole burning [Mel05]. In general this technique uses a high-intensity laser of frequency ω_L to optically pump any ions that have a transition resonant with ω_L to an auxiliary long-lived ground state. This results in the medium becoming temporarily transparent to light of frequency ω_L. By scanning the laser frequency over a range of values, broader transparency windows can be created. In order to prepare the medium for the CRIB protocol, a narrow peak is left in the middle of the wider transparency window, as depicted in Figure 3.1(b). Finally, this line is broadened via an externally applied electric field, $\mathbf{E}_\mathrm{S}$, that results in a Stark

shift of each ion. Due to either the random nature of local stresses and strains within an amorphous medium, or a gradient in the applied field for the case of crystals, the absorption frequency resulting from the Stark shift will not be the same for each ion. The net effect is an inhomogeneously broadened spectrum as shown in Figure 3.1(c).

With this setup the CRIB protocol can now be implemented. When the absorption profile is artificially broadened, the photon to be stored is sent into the medium. It will be absorbed and the atoms will begin to dephase with respect to each other. Reversing the polarity of the externally applied field, $\mathbf{E}_{\mathrm{S}} \rightarrow -\mathbf{E}_{\mathrm{S}}$, will cause the Stark shift affecting each ion to also be negated. That is, ions initially detuned by an amount Δ will be detuned by $-\Delta$ after reversing the field; the collective effect of this over all ions is to transform $g(\Delta) \rightarrow g(-\Delta)$. A frequently-proposed method for applying the $2kz$ phase shift to the ensemble is to apply two counter-propagating π pulses to the medium, transferring the excited atomic population to an auxiliary long-lived ground state and back. Once the detunings have been reversed and the phase shift applied, the atoms will begin rephasing, resulting in the photon re-emerging from the medium.

3.2.1 Tranverse vs. longitudinal broadening

The absorption profiles referred to here, particularly those in Figure 3.1, describe how the memory medium as a whole absorbs light. There are two distinct ways in which one can obtain such profiles over a finite length. One method is to create a single absorption peak at each position z between 0 and L, so that the entire width of the profile $g(\Delta)$ is only seen when considering the full length of the medium. This results in a position-dependent distribution such as

$$g(\Delta, z) = \delta\left[\Delta - \gamma\left(\frac{z}{L} - \frac{1}{2}\right)\right] \ , \tag{3.8}$$

which states that the resonance frequency in the medium varies linearly from $-\gamma/2$ at $z = 0$ to $\gamma/2$ at $z = L$. Such a distribution is often called 'longitudinal broadening' since

the profile is only broad when integrated along the propagation direction. This method has been explored both theoretically and experimentally by the research group of Matt Sellars in Australia [HLA+08].

The other option occurs if at each position within the medium, which has finite width, there exist multiple absorbers such that the entire profile $g(\Delta)$ is present at each z. Such a position-independent distribution is termed 'transverse broadening' due to the fact that the variation in the profile occurs transverse to the direction of propagation. It was this type of distribution which was assumed in the initial proposal for a CRIB-based memory [MK01], and is the subject of the current work. While currently being attempted in at least two research laboratories, the CRIB protocol based on transverse broadening has yet to be implemented experimentally.

3.3 Analysis of CRIB

Some initial assumptions about the pulse that we wish to store, $\Omega_{\mathrm{f}}(0,t)$, must be made. Clearly the pulse must be assumed to have a finite duration if one expects to store it in its entirety. In order for decoherence effects to be minimized it is further assumed that the temporal full-width-at-half-maximum duration of the pulse, δt, is short compared to T_2, the inverse of the optical linewidth. These assumptions imply that the pulse is localized in time, and it is useful to define t_p as the temporal centre of the pulse.

3.3.1 Forward direction

The equations (3.1) and (3.2) that exhibit perfect time reversal symmetry represent the ideal case of unitary evolution within the system. In reality decoherence effects including spontaneous emission break unitarity. This can be included in the model of the system

via inclusion of the decoherence rate,

$$\Gamma_2 = \frac{1}{\pi T_2} \ . \tag{3.9}$$

In this case the evolution of the atomic polarization can be stated as

$$\partial_t \sigma_i(z,t,\Delta) = (\mathrm{i}\Delta - \Gamma_2)\,\sigma_i(z,t,\Delta) + \mathrm{i}\Omega_i(z,t) \ , \tag{3.10}$$

for $i \in \{\mathrm{f},\mathrm{b}\}$. The goal here will be to assume that an input pulse at the start of the medium has a known temporal shape, $\Omega_\mathrm{f}(0,t)$, and to determine the behaviour of the light plus atoms as the protocol is performed.

In the work of Sangouard *et al.* [SSAG07], a similar analysis was performed, but with the assumption of infinite coherence times, $\Gamma_2 = 0$. The methods employed in these sections are motivated by their work, with the added inclusion of a non-zero decay rate. The first step is to formally integrate the evolution equation (3.10) to find a solution for σ_f under the assumption that all atoms are initially in the ground state so that $\sigma_\mathrm{f}(z,-\infty,\Delta) = 0$. This solution,

$$\sigma_\mathrm{f}(z,t,\Delta) = \mathrm{i}\int_{-\infty}^{t} \mathrm{d}s\, \mathrm{e}^{(\mathrm{i}\Delta-\Gamma_2)(t-s)}\Omega_\mathrm{f}(z,s) \ , \tag{3.11}$$

turns the paraxial wave equation into

$$\left(\frac{n}{c}\partial_t + \partial_z\right)\Omega_\mathrm{f} = -\beta\int_{-\infty}^{\infty}\mathrm{d}\Delta\, g(\Delta)\int_{-\infty}^{t}\mathrm{d}s\, \mathrm{e}^{(\mathrm{i}\Delta-\Gamma_2)(t-s)}\Omega_\mathrm{f}(z,s) \ . \tag{3.12}$$

Taking the Fourier transform of this partial differential equation (PDE) will turn it into an ordinary differential equation (ODE) that will be easier to solve. The transformation results in

$$\left(\mathrm{i}\frac{n\omega}{c} + \partial_z\right)\tilde{\Omega}_\mathrm{f}(z,\omega) = \frac{-\beta}{\sqrt{2\pi}}\int_{-\infty}^{\infty}\mathrm{d}\Delta\, g(\Delta)\int_{-\infty}^{\infty}\mathrm{d}t\, \mathrm{e}^{-\mathrm{i}\omega t}\int_{-\infty}^{t}\mathrm{d}s\, \mathrm{e}^{(\mathrm{i}\Delta-\Gamma_2)(t-s)}\Omega_\mathrm{f}(z,s) \ . \tag{3.13}$$

Next, the order of integration over the s-t plane is reversed, and the variable $u = t - s$ is introduced. This isolates the Fourier transform of the input field and yields an integral

which can be evaluated:

$$\left(\mathrm{i}\frac{n\omega}{c}+\partial_z\right)\tilde{\Omega}_\mathrm{f}(z,\omega)=\frac{-\beta}{\sqrt{2\pi}}\int_{-\infty}^{\infty}\mathrm{d}\Delta\, g(\Delta)\int_{-\infty}^{\infty}\mathrm{d}s\,\Omega_\mathrm{f}(z,s)\int_{s}^{\infty}\mathrm{d}t\,\mathrm{e}^{-\mathrm{i}\omega t}\mathrm{e}^{(\mathrm{i}\Delta-\Gamma_2)(t-s)} \tag{3.14a}$$

$$=\frac{-\beta}{\sqrt{2\pi}}\int_{-\infty}^{\infty}\mathrm{d}\Delta\, g(\Delta)\int_{-\infty}^{\infty}\mathrm{d}s\,\Omega_\mathrm{f}(z,s)\int_{0}^{\infty}\mathrm{d}u\,\mathrm{e}^{-\mathrm{i}\omega(u+s)}\mathrm{e}^{(\mathrm{i}\Delta-\Gamma_2)u} \tag{3.14b}$$

$$=-\beta\int_{-\infty}^{\infty}\mathrm{d}\Delta\, g(\Delta)\tilde{\Omega}_\mathrm{f}(z,\omega)\int_{0}^{\infty}\mathrm{d}u\,\mathrm{e}^{\mathrm{i}(\Delta-\omega)u}\mathrm{e}^{-\Gamma_2 u}\ . \tag{3.14c}$$

Due to the assumption that Γ_2 is positive, the integral over u converges. This leaves an ODE with respect to z,

$$\left(\mathrm{i}\frac{n\omega}{c}+\partial_z\right)\tilde{\Omega}_\mathrm{f}(z,\omega)=-\beta\int_{-\infty}^{\infty}\mathrm{d}\Delta\,\frac{g(\Delta)}{\Gamma_2-\mathrm{i}(\Delta-\omega)}\tilde{\Omega}_\mathrm{f}(z,\omega)\ . \tag{3.15}$$

A function of ω is defined to be this integral over Δ in order to simplify the notation of the previous expression,

$$H(\omega):=\int_{-\infty}^{\infty}\mathrm{d}\Delta\,\frac{g(\Delta)}{\Gamma_2-\mathrm{i}(\Delta-\omega)}\ , \tag{3.16}$$

so that the evolution of the Fourier components of the incoming light field can be seen to evolve according to

$$\partial_z\tilde{\Omega}_\mathrm{f}(z,\omega)=-\left(\mathrm{i}\frac{n\omega}{c}+\beta H(\omega)\right)\tilde{\Omega}_\mathrm{f}(z,\omega)\ . \tag{3.17}$$

This homogeneous DE is easily solved by

$$\tilde{\Omega}_\mathrm{f}(z,\omega)=\mathrm{e}^{-\mathrm{i}n\omega z/c}\mathrm{e}^{-\beta H(\omega)z}\tilde{\Omega}_\mathrm{f}(0,\omega)\ , \tag{3.18}$$

from which an absorption coefficient can be determined. The intensity of each frequency component decreases exponentially with distance into the medium,

$$\frac{|\Omega_\mathrm{f}(z,\omega)|^2}{|\Omega_\mathrm{f}(0,\omega)|^2}=\mathrm{e}^{-2\beta\mathrm{Re}[H(\omega)]z}\ . \tag{3.19}$$

This leads to the definition of the absorption coefficient

$$\alpha(\omega) := 2\beta \mathrm{Re}\left[H(\omega)\right] \ . \tag{3.20}$$

Note that $g(\Delta)$, β, and Γ_2 are all positive by definition. Thus α is also positive, as it must be to describe an absorbing medium, since

$$\mathrm{Re}\left[H(\omega)\right] = \int_{-\infty}^{\infty} \mathrm{d}\Delta \, \frac{g(\Delta)\Gamma_2}{\Gamma_2^2 + (\Delta - \omega)^2} > 0 \ . \tag{3.21}$$

3.3.2 Backward direction

Since the medium absorbing the pulse is of finite length L, a time T_0 can be chosen at which no non-negligible portiton of the pulse remains within the medium. There is of course no backward-moving field at this time either, so it can be safely assumed that $\Omega_\mathrm{f}(z, T_0) = \Omega_\mathrm{b}(z, T_0) = 0$. This time is taken to be the moment at which the detunings are reversed, $g(\Delta) \to g(-\Delta)$, and a $2kz$ phase shift is applied so that $\sigma_\mathrm{f} \to \sigma_\mathrm{b}$. The state of the polarization at $t = T_0$ is given by

$$\sigma_\mathrm{b}(z, T_0, \Delta) = \sigma_\mathrm{f}(z, T_0, -\Delta) = \mathrm{i} \int_{-\infty}^{T_0} \mathrm{d}s \, \mathrm{e}^{-(i\Delta + \Gamma_2)(T_0 - s)} \Omega_\mathrm{f}(z, s) =: \sigma_0(z, \Delta) \ . \tag{3.22}$$

After the detunings have been reversed, the equations of motion for the backward-moving field are given by

$$\left(\frac{n}{c}\partial_t - \partial_z\right) \Omega_\mathrm{b}(z, t) = \mathrm{i}\beta \int_{-\infty}^{\infty} \mathrm{d}\Delta \, g(\Delta) \sigma_\mathrm{b}(z, t, \Delta) \ ,$$

$$\partial_t \sigma_\mathrm{b}(z, t, \Delta) = (\mathrm{i}\Delta - \Gamma_2)\sigma_\mathrm{b}(z, t, \Delta) + \mathrm{i}\Omega_\mathrm{b}(z, t) \ .$$

The polarization is again solved for formally,

$$\sigma_\mathrm{b}(z, t, \Delta) = \sigma_0(z, \Delta) \mathrm{e}^{(\mathrm{i}\Delta - \Gamma_2)(t - T_0)} + \mathrm{i} \int_{T_0}^{t} \mathrm{d}s \, \mathrm{e}^{(\mathrm{i}\Delta - \Gamma_2)(t - s)} \Omega_\mathrm{b}(z, s) \ . \tag{3.23}$$

Putting this into the paraxial wave equation for the light field results in

$$\left(\frac{n}{c}\partial_t - \partial_z\right) \Omega_\mathrm{b}(z, t) = \mathrm{i}\beta \int_{-\infty}^{\infty} \mathrm{d}\Delta \, g(\Delta) \sigma_0 \mathrm{e}^{(\mathrm{i}\Delta - \Gamma_2)(t - T_0)}$$
$$- \beta \int_{-\infty}^{\infty} \mathrm{d}\Delta \, g(\Delta) \int_{T_0}^{t} \mathrm{d}s \, \mathrm{e}^{(\mathrm{i}\Delta - \Gamma_2)(t - s)} \Omega_\mathrm{b}(z, s) \ . \tag{3.24}$$

As in the previous section the next step will be to Fourier transform this equation. The left-hand side and second term on the right-hand side are very similar to (3.12), and the applicable methods are likewise similar. The additional term in this equation provided by the non-zero initial condition for σ_0 is worth investigating more closely. In order to relate it to the input pulse, the definition (3.22) is used along with the Fourier transform, resulting in

$$\begin{aligned}&\frac{\mathrm{i}\beta}{\sqrt{2\pi}}\int_{-\infty}^{\infty}\mathrm{d}\Delta\, g(\Delta)\mathrm{e}^{-(\mathrm{i}\Delta-\Gamma_2)T_0}\int_{-\infty}^{\infty}\mathrm{d}t\,\mathrm{e}^{-\mathrm{i}\omega t}\mathrm{e}^{(\mathrm{i}\Delta-\Gamma_2)t}\sigma_0\\ &\quad=\frac{-\beta}{\sqrt{2\pi}}\int_{-\infty}^{\infty}\mathrm{d}\Delta\, g(\Delta)\mathrm{e}^{-2\mathrm{i}\Delta T_0}\int_{-\infty}^{\infty}\mathrm{d}t\int_{-\infty}^{\infty}\mathrm{d}s\,\mathrm{e}^{-\mathrm{i}\omega t}\mathrm{e}^{\mathrm{i}\Delta(t+s)}\mathrm{e}^{\Gamma_2(s-t)}\Omega_\mathrm{f}(z,s)\ .\end{aligned}\tag{3.25}$$

This time a useful substitution is provided by $u=t+s$, which turns (3.25) into

$$\frac{-\beta}{\sqrt{2\pi}}\int_{-\infty}^{\infty}\mathrm{d}\Delta\, g(\Delta)\mathrm{e}^{-2\mathrm{i}\Delta T_0}\int_{-\infty}^{\infty}\mathrm{d}u\int_{-\infty}^{\infty}\mathrm{d}s\,\mathrm{e}^{-\mathrm{i}\omega(u-s)}\mathrm{e}^{\mathrm{i}\Delta u}\mathrm{e}^{\Gamma_2(2s-u)}\Omega_\mathrm{f}(z,s)\tag{3.26a}$$

$$=\frac{-\beta}{\sqrt{2\pi}}\int_{-\infty}^{\infty}\mathrm{d}\Delta\, g(\Delta)\mathrm{e}^{-2\mathrm{i}\Delta T_0}\int_{-\infty}^{\infty}\mathrm{d}u\,\mathrm{e}^{-\mathrm{i}\omega u}\mathrm{e}^{\mathrm{i}\Delta u}\mathrm{e}^{-\Gamma_2 u}\int_{-\infty}^{\infty}\mathrm{d}s\,\mathrm{e}^{-\mathrm{i}(-\omega+2\mathrm{i}\Gamma_2)s}\Omega_\mathrm{f}(z,s)\tag{3.26b}$$

$$=-\beta\tilde{\Omega}_\mathrm{f}(z,-\omega+2\mathrm{i}\Gamma_2)\int_{-\infty}^{\infty}\mathrm{d}u\,\mathrm{e}^{-(\mathrm{i}\omega+\Gamma_2)u}\int_{-\infty}^{\infty}\mathrm{d}\Delta\, g(\Delta)\mathrm{e}^{\mathrm{i}\Delta(u-2T_0)}\ .\tag{3.26c}$$

In order to simplify notation again the terms independent of z are grouped into the definition of a new function,

$$F(\omega):=\int_{-\infty}^{\infty}\mathrm{d}u\,\mathrm{e}^{-(\mathrm{i}\omega+\Gamma_2)u}\int_{-\infty}^{\infty}\mathrm{d}\Delta\, g(\Delta)\mathrm{e}^{\mathrm{i}\Delta(u-2T_0)}\ ,\tag{3.27}$$

and the solution (3.18) for $\tilde{\Omega}_\mathrm{f}$ can then be used to continue from (3.26c) with

$$-\beta F(\omega)\tilde{\Omega}_\mathrm{f}(z,-\omega+2\mathrm{i}\Gamma_2)=-\beta F(\omega)\mathrm{e}^{-\mathrm{i}n(-\omega+2\mathrm{i}\Gamma_2)z/c}\mathrm{e}^{-\beta H(-\omega+2\mathrm{i}\Gamma_2)z}\tilde{\Omega}_\mathrm{f}(0,-\omega+2\mathrm{i}\Gamma_2)\ .\tag{3.28}$$

Combined with the Fourier transform of the rest of (3.24), this result yields the following equation of motion:

$$\begin{aligned}\partial_z\tilde{\Omega}_\mathrm{b}(z,\omega)=&\left(\mathrm{i}\frac{n\omega}{c}+\beta H(\omega)\right)\tilde{\Omega}_\mathrm{b}(z,\omega)\\ &+\beta F(\omega)\mathrm{e}^{\mathrm{i}\omega nz/c}\mathrm{e}^{2\Gamma_2 nz/c}\mathrm{e}^{-\beta H(-\omega+2\mathrm{i}\Gamma_2)z}\tilde{\Omega}_\mathrm{f}(0,-\omega+2\mathrm{i}\Gamma_2)\ .\end{aligned}$$

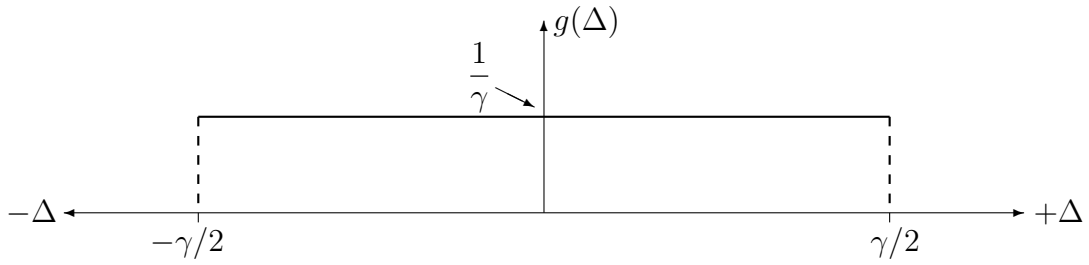

Figure 3.2: The uniform distribution of detunings. The integral of this $g(\Delta)$ over all Δ evaluates to unity.

By assumption there is no backward-moving electric field approaching the storage medium from $z > L$. This provides the boundary condition $\tilde{\Omega}_{\mathrm{b}}(L, \omega) = 0$, under which the solution for the frequency component is given by

$$\tilde{\Omega}_{\mathrm{b}}(z,\omega) = \beta F(\omega)\tilde{\Omega}_{\mathrm{f}}(0, -\omega + 2\mathrm{i}\Gamma_2)\mathrm{e}^{-\beta L H(\omega) - \beta(L+z)H(-\omega+2\mathrm{i}\Gamma_2)}\mathrm{e}^{\mathrm{i}\omega n z/c} \times \frac{\mathrm{e}^{\beta z[H(\omega)+H(-\omega+2\mathrm{i}\Gamma_2)]+2\Gamma_2 nL/c} - \mathrm{e}^{\beta L[H(\omega)+H(-\omega+2\mathrm{i}\Gamma_2)]+2\Gamma_2 nz/c}}{\beta[H(\omega)+H(-\omega+2\mathrm{i}\Gamma_2)] - 2\Gamma_2 n/c} . \quad (3.29)$$

Short of noting that there is dependence on the input pulse through $\tilde{\Omega}_{\mathrm{f}}(0, \omega)$ there is little more that can be done at this point, since without knowledge of $g(\Delta)$ the functions $F(\omega)$ and $H(\omega)$ cannot be evaluated. Some physical meaning of this result will be discussed in Section 3.5 when the recall efficiency due to a specific form for $g(\Delta)$ is investigated.

3.4 Specific cases

In order to proceed much further with this analysis the form of the distribution of detunings, $g(\Delta)$, must be specified. It will be assumed that the detuning profile can be characterized by some full-width $\gamma > 0$, such that all non-negligible frequency components will fall within the width of g. That is, $\gamma \gg \omega$ (recalling that while working in the rotating frame $\omega = 0$ corresponds to light at the central atomic resonance). Furthermore it will be assumed that while the excited-state lifetime is not infinite, the state is

long-lived so that $\gamma \gg \Gamma_2$.

A physically realistic description of the distribution $g(\Delta)$ is perhaps provided by a Gaussian or Lorentzian function. A function that is simple to deal with mathematically in many of the integrals involved is the uniform distribution which takes on a constant positive value within a given range and vanishes everywhere else. It can be shown that under approximations due to the stated assumptions, these three distributions yield values of $H(\omega)$ that differ only by constant factors. For a given width γ and physical system characterized by β, the uniform distribution attenuates the input pulse more quickly than the Lorentzian, which in turn absorbs more strongly than the Gaussian distribution, but otherwise their behaviours are the same. In fact, for any sufficiently wide and smooth distribution g, the value of $g(\Delta)$ can be approximated by $g(0)$ for those Δ that contribute significantly to the behaviour of the system. Therefore *any* distribution that satisfies this set of assumptions will result in an absorption coefficient independent of ω, and differing from α only by a constant factor. For this reason it is sufficient to consider only the uniform distribution from now on, as is common practice.

3.4.1 The uniform distribution

The previously described uniform distribution, shown in Figure 3.2, can be described mathematically as

$$g(\Delta) = \frac{1}{\gamma}\Theta\left(\frac{\gamma}{2} + \Delta\right)\Theta\left(\frac{\gamma}{2} - \Delta\right) \ . \tag{3.30}$$

This states that the frequencies of the atoms are uniformly distributed within a window of width γ centred on ω_0 (i.e. on $\Delta = 0$), and that no atoms exist with detunings outside that range.

In this case $H(\omega)$ as defined in (3.16) evaluates to

$$H(\omega) = \frac{2}{\gamma}\arctan\left(\frac{\gamma}{2}\frac{1}{\Gamma_2 + \mathrm{i}\omega}\right) \ . \tag{3.31}$$

Under the given assumptions, $\gamma \gg |\Gamma_2 + \mathrm{i}\omega|$ and the argument of arctan is sufficiently large to approximate

$$H(\omega) \approx \frac{\pi}{\gamma} \quad \Longrightarrow \quad \alpha = \frac{2\beta\pi}{\gamma} \ . \tag{3.32}$$

The Fourier components of the light field then decay according to (3.18),

$$\tilde{\Omega}_{\mathrm{f}}(z,\omega) = \mathrm{e}^{-\beta\pi z/\gamma}\mathrm{e}^{-\mathrm{i}\omega n z/c}\tilde{\Omega}_{\mathrm{f}}(0,\omega) \ , \tag{3.33}$$

which shows that as the field propagates into the medium it evolves as

$$\Omega_{\mathrm{f}}(z,t) = \mathrm{e}^{-\alpha z/2}\Omega_{\mathrm{f}}(0, t - nz/c) \ . \tag{3.34}$$

This is easily interpreted as follows: The pulse moves through the medium in the positive z direction with speed c/n; as it does so it retains its original shape, while its amplitude decays exponentially.

3.4.2 The Gaussian distribution

As already mentioned there is little need to investigate other distributions so long as the assumptions about their general form are satisfied. It is however informative to show explicitly that this is true for at least one other case, so in this brief subsection a moment will be taken to see the effect of choosing to work with the Gaussian distribution,

$$g_{\mathrm{G}}(\Delta) = \frac{\mathrm{e}^{-\Delta^2/2\gamma^2}}{\gamma\sqrt{2\pi}} \ . \tag{3.35}$$

The resulting form of $H(\omega)$ is again able to be solved exactly,

$$H_{\mathrm{G}}(\omega) = \frac{1}{\gamma}\sqrt{\frac{\pi}{2}}\mathrm{e}^{(\Gamma_2+\mathrm{i}\omega)^2/2\gamma^2}\mathrm{erfc}\left(\frac{\Gamma_2 + \mathrm{i}\omega}{\gamma\sqrt{2}}\right) \approx \frac{1}{\gamma}\sqrt{\frac{\pi}{2}} \ , \tag{3.36}$$

where the final approximation again makes use of the fact that $\gamma \gg |\Gamma_2 + \mathrm{i}\omega|$. The absorption coefficient is then found from (3.20) to be

$$\alpha_{\mathrm{G}} = \frac{2\beta}{\gamma}\sqrt{\frac{\pi}{2}} = \frac{\alpha}{\sqrt{2\pi}} \ . \tag{3.37}$$

The reason for this can be easily seen from the assumption that the pulse is much narrower in frequency space than the distribution of detunings. In this case most interaction occurs roughly at the centre of the distribution; and it is clear to see that

$$g_{\mathrm{G}}(0) = \frac{g(0)}{\sqrt{2\pi}} \ . \tag{3.38}$$

The absorption coefficients reflect this accordingly.

3.5 Recall efficiency

Of particular interest in any memory, quantum or otherwise, is the ability to recall what has been stored. In this case what is being stored is the input light pulse, $\Omega_{\mathrm{f}}(0,t)$, and the field recalled from the medium is likewise $\Omega_{\mathrm{b}}(0,t)$. From (3.29) it can be seen that

$$\tilde{\Omega}_{\mathrm{b}}(0,\omega) = \frac{\beta F(\omega)\mathrm{e}^{-\beta L[H(\omega)+H(-\omega+2\mathrm{i}\Gamma_2)]}\left(\mathrm{e}^{2\Gamma_2 nL/c} - \mathrm{e}^{\beta L[H(\omega)+H(-\omega+2\mathrm{i}\Gamma_2)]}\right)}{\beta[H(\omega)+H(-\omega+2\mathrm{i}\Gamma_2)] - 2\Gamma_2 n/c}\tilde{\Omega}_{\mathrm{f}}(0,-\omega+2\mathrm{i}\Gamma_2) \ . \tag{3.39}$$

This is still not particularly enlightening, and it is again useful to turn to the uniform distribution for further analysis. As already seen, in the case of large γ the function H can be approximated by $H(\omega) \approx \pi/\gamma$. Similarly it can be shown that in the same regime $F(\omega)$ can be approximated by

$$F(\omega) \approx \frac{2\pi}{\gamma}\mathrm{e}^{-2\mathrm{i}\omega T_0}\mathrm{e}^{-2\Gamma_2 T_0} \ . \tag{3.40}$$

With these approximations the expression for the Fourier components reduces to

$$\tilde{\Omega}_{\mathrm{b}}(0,\omega) = \frac{1-\mathrm{e}^{2\Gamma_2 nL/c - 2\beta\pi L/\gamma}}{1-\Gamma_2\gamma n/c\beta\pi}\mathrm{e}^{-2(\mathrm{i}\omega+\Gamma_2)T_0}\tilde{\Omega}_{\mathrm{f}}(0,-\omega+2\mathrm{i}\Gamma_2) \ . \tag{3.41}$$

The inverse Fourier transform of this expression will finally yield an expression for the output pulse recalled from the medium. After defining the constant

$$\eta := \Gamma_2\frac{\gamma n}{\pi\beta c} \ , \tag{3.42}$$

and recalling that the absorption coefficient for the medium is given by $\alpha = 2\beta\pi/\gamma$, the output pulse given by the inverse Fourier transform of (3.41) can be written as

$$\Omega_{\mathrm{b}}(0,t) = -\mathrm{e}^{-2\Gamma_2(t-T_0)}\frac{1-\mathrm{e}^{-\alpha L(1-\eta)}}{1-\eta}\Omega_{\mathrm{f}}(0,-t+2T_0)\ . \tag{3.43}$$

Note that in the case of atoms with infinite excited-state lifetimes, $\Gamma_2 = 0$ ($\implies \eta = 0$), and with the recall being initiated at $T_0 = 0$, this simplifies to

$$\Omega_{\mathrm{b}}(0,t) = -\left(1-\mathrm{e}^{-\alpha L}\right)\Omega_{\mathrm{f}}(0,-t)\ . \tag{3.44}$$

The simplified result (3.44) is in agreement with the previous work of Sangouard *et al.* describing the ideal case [SSAG07]. The new extension to their work resulting from the less-ideal case described by (3.43) is analyzed here in further detail.

3.5.1 The magnitude of η

While Γ_2 has been kept finite throughout this analysis, it has been assumed that the effects of decoherence are small; if they weren't, no coherent storage of light could be performed. Therefore it should be expected that the denominator in (3.43) is roughly equal to unity. However, this cannot be guaranteed based solely on the stated assumptions, since $\gamma \gg \Gamma_2$ says nothing about the product $\Gamma_2\gamma$. Furthermore the other terms involved, such as β, depend only on the physical system involved and no mathematical assumptions have been made about them.

Before investigating the output pulse specified in (3.43) further, it will be shown that the statement $\eta \ll 1$ is valid in at least one important case for QKD implementations, that of Erbium-doped silicate optical fibres, with values taken again from the work of Staudt [Sta08]. Using the definition of β, the dimensionless constant η is seen to be

$$\eta = \Gamma_2\frac{\gamma n}{\pi c}\frac{2\epsilon_0\hbar n c}{\omega_L N \wp^2} = \frac{2\Gamma_2\epsilon_0\gamma\hbar n^2}{\pi\omega_L N\wp^2}\ . \tag{3.45}$$

Experimental results give a value of $\wp/\hbar \sim 50$ Hz m/V so that

$$\frac{\hbar}{\wp^2} \approx 6 \times 10^{29} \frac{\mathrm{V^2 s}}{\mathrm{m^2 J}} \ . \tag{3.46}$$

The magnitude of Γ_2 has a strong dependence on temperature; for an Erbium-doped glass at 150 mK it is on the order of 10^5 Hz. The dopant density can vary over several orders of magnitude, and is typically between 10^{23} and 10^{27} $\mathrm{m^{-3}}$; consider the median, $N \sim 10^{25}$ $\mathrm{m^{-3}}$. Typical telecommunication wavelengths are on the order of 1000 nm, which translates to $\omega_L \approx 5 \times 10^{13}$ $\mathrm{s^{-1}}$. Combining these values with those of the fundamental constants involved and a refractive index of $n = 1.5$ results in $\eta \sim \gamma \times (10^{-15}$ s). To store a 10 ns pulse the medium must be able to accommodate a spectral width on the order of 100 MHz, so to satisfy the assumption that the linewidth of the medium is greater than the bandwidth of the photon, γ should be on the order of 1 GHz. This finally results in an order-of-magnitude approximation,

$$\eta \sim 10^{-6} \ , \tag{3.47}$$

which is indeed small as compared with unity.

3.5.2 Analysis of the recalled pulse

The opposite signs of Ω_b and Ω_f indicate that the pulse acquires an overall π phase shift during storage in the memory, while the argument of $-t + 2T_0$ to Ω_f shows that the temporal shape of the output Ω_b is a reflection of the input pulse shape about the time $t = T_0$. It is this fact which proves the claim that the medium has in fact acted as a memory to store the light pulse.

The remaining term of interest is the prefactor

$$\chi(t) := \mathrm{e}^{-2\Gamma_2(t-T_0)} \frac{1 - \mathrm{e}^{-\alpha L(1-\eta)}}{1-\eta} \ . \tag{3.48}$$

Since $0 < \eta \ll 1$ it is clear that $\chi(t)$ is always positive, so the phase of the output is unaffected by this term. As expected from the physical nature of the decay rate Γ_2, the amplitude of the recalled pulse decreases exponentially with the storage time. Furthermore, the original shape of the pulse is damped by the decay term. However, it is assumed that the excited-state lifetime is much longer than the storage duration, which is in turn longer than the pulse width. Therefore the magnitude of the decay term is roughly constant over the width of the pulse, so that the shape is only negligibly affected and the decay term can be replaced by its value at the peak of the pulse, $t = -t_p + 2T_0$,

$$\mathrm{e}^{-2\Gamma_2(t-T_0)} \approx \mathrm{e}^{-2\Gamma_2(T_0-t_p)} \ . \tag{3.49}$$

This results in $\chi(t)$ being redefined as a constant effective scaling factor for the recalled pulse, given by

$$\chi := \mathrm{e}^{-2\Gamma_2(T_0-t_p)} \frac{1-\mathrm{e}^{-\alpha L(1-\eta)}}{1-\eta} \ . \tag{3.50}$$

Expanding the fraction in (3.48) to first-order in η results in

$$\frac{1-\mathrm{e}^{-\alpha L(1-\eta)}}{1-\eta} = 1 - \mathrm{e}^{-\alpha L} - \eta \mathrm{e}^{-\alpha L}(1+\alpha L) + \eta + \mathcal{O}\left(\eta^2\right) \ . \tag{3.51}$$

For very large optical depth, $\alpha L \gg 1$, this is roughly equal to $1+\eta$, which appears to imply that the amplitude of the output pulse is actually *greater* than that of the input. However, note that for χ to exceed unity in this regime it is required that t_p be very close to T_0 so that $1 + \eta > \mathrm{e}^{2\Gamma_2(T_0-t_p)}$, or

$$2\Gamma_2(T_0 - t_p) < \ln(1+\eta) \approx \eta \quad \Longrightarrow \quad 2(T_0 - t_p) \lessapprox \frac{\eta}{\Gamma_2} \ . \tag{3.52}$$

It has been seen though that a typical value for η/Γ_2 is on the order of 10^{-11} s. This is small even compared to the temporal duration of pulses that may be stored, and the storage time, $\delta t := 2(T_0 - t_p)$, is expected to be closer to microseconds or even milliseconds. Therefore it may be the case that $\chi > 1$ for the first few hundredths of a

nanosecond or so of the recall stage, but the field that it would be amplifying at those times is essentially zero.

It can be concluded then that for arbitrary optical depth, the factor χ will lie in the range $[0, 1]$ at all times for which the ideal recalled field, $\Omega_{\rm f}(0, -t+2T_0)$, is non-negligible.

3.5.3 Phase of the recalled field

The expression (3.29) describes only the Fourier components of the envelope of the recalled field, $\tilde{\Omega}_{\rm b}(0, \omega)$. While the field $\Omega_{\rm b}(0, t)$ cannot be calculated in general as mentioned above, something can be said about the phase relationship between its peak and that of the input pulse. Assuming that for a specific case one has found $\Omega_{\rm b}(0, t)$, the actual electric field emitted from the medium is described by (for $t_{\rm b} > T_0$)

$$E(0, t_{\rm b}) = \frac{\hbar\Omega_{\rm b}(0, t_{\rm b})}{2\wp} {\rm e}^{-{\rm i}\omega_L t_{\rm b}} + {\rm c.c.} \tag{3.53}$$

On the other hand, the electric field at the front of the medium for times $t_{\rm f} < T_0$ is given by

$$E(0, t_{\rm f}) = \frac{\hbar\Omega_{\rm f}(0, t_{\rm f})}{2\wp} {\rm e}^{-{\rm i}\omega_L t_{\rm f}} + {\rm c.c.} \tag{3.54}$$

Consider then the phase difference between the fields at their peaks, temporally located at $t_{\rm f} = t_p$ and $t_{\rm b} = -t_p + 2T_0$:

$$\delta\varphi = \omega_L[(-t_p + 2T_0) - t_p] = \omega_L 2(T_0 - t_p) = \omega_L\, \delta t\ . \tag{3.55}$$

This provides a method for controlling the relative phase of the output pulse. Suppose for example that two in-phase pulses are stored and then recalled, one after the other. If the first is stored for a duration δt and the second for $\delta t + \pi/\omega_L$ then the two recalled pulses will be out of phase by π.

3.5.4 Output energy

A useful definition for the recall efficiency of a memory is given by the percentage of the total input energy that is recalled. Define

$$E_{\mathrm{f}} := \int_{-\infty}^{T_0} \mathrm{d}t \ |\Omega_{\mathrm{f}}(0,t)|^2 \ , \tag{3.56}$$

which is proportional to the total energy sent into the memory medium. Similarly, the output energy should then be defined by

$$E_{\mathrm{b}} := \int_{T_0}^{\infty} \mathrm{d}t \ |\Omega_{\mathrm{b}}(0,t)|^2 \ . \tag{3.57}$$

The efficiency as defined is then simply

$$\mu := \frac{E_{\mathrm{b}}}{E_{\mathrm{f}}} \ . \tag{3.58}$$

These two energies can be related by making use of the solution (3.43) for the output pulse, modified to include the term χ as defined in (3.50), to write

$$E_{\mathrm{b}} = \chi^2 \int_{T_0}^{\infty} \mathrm{d}t \ |\Omega_{\mathrm{f}}(0,-t+2T_0)|^2 = \chi^2 \int_{-\infty}^{T_0} \mathrm{d}t \ |\Omega_{\mathrm{f}}(0,t)|^2 = \chi^2 E_{\mathrm{f}} \ . \tag{3.59}$$

Therefore, based on the definition of χ, the memory's recall efficiency is

$$\mu = \chi^2 = \mathrm{e}^{-4\Gamma_2(T_0-t_p)} \left(\frac{1-\mathrm{e}^{-\alpha L(1-\eta)}}{1-\eta} \right)^2 \ . \tag{3.60}$$

3.5.5 The ideal case

In order to examine the ideal scenario one can neglect decoherence effects by setting $\Gamma_2 = 0$. This is a good approximation to the physical system when the coherence time $1/\Gamma_2$ is much longer than the storage time, $\delta t = 2(T_0 - t_p)$. This statement results in a further approximation,

$$1 \gg 2\Gamma_2(T_0 - t_p) \quad \Longrightarrow \quad \mathrm{e}^{-4\Gamma_2(T_0-t_p)} \approx 1 \ . \tag{3.61}$$

Of course, for the ideal case $\Gamma_2 = 0$ this exponential equals unity exactly. Under these assumptions the recall efficiency simplifies to

$$\mu = \left(1 - \mathrm{e}^{-\alpha L}\right)^2 \ . \tag{3.62}$$

This again agrees with the results of [SSAG07], and can be easily seen from the expression for the field recalled in the ideal case, (3.44). Under the common assumption of large optical depth, $\alpha L \gg 1$, the value of μ tends to unity. That is, perfect recall is achieved.

Chapter 4

Breaking time-reversal symmetry

It has been shown that not every aspect of the CRIB protocol described in Chapter 3 is required in order to recall the pulse from the medium, although modifying the protocol tends to result in a decrease in efficiency. For example, if the $2kz$ phase shift is not applied when the detunings are reversed then the pulse will still be recalled from the medium, and will come out propagating in the forward direction [SSAG07]. Without this phase shift the equations of motion do not exhibit perfect time-reversal symmetry, so the recall is not 100% efficient, in the same way that the decoherence effects due to non-zero Γ_2 both break the symmetry and decrease the memory's efficiency. It could be imagined then that there may be other ways in which the symmetry of the system could be broken, yet still allow at least partial recall of the stored pulse. Indeed, it is exactly this effect that is exploited in the current chapter to allow a single temporally localized input pulse to be transformed into a pair of temporally separated pulses, each with the same shape as the input, albeit with smaller amplitudes. This results in the medium performing the same function as a beam splitter, although the beam is split into different temporal modes rather than different spatial modes as with a standard beam splitter. A method for applying an arbitrarily chosen phase to one of the beam splitter's outputs is also described.

The resulting decrease in efficiency could prevent this scheme from being useful in a setting that requires it to be used repeatedly on a single qubit, for example as a single-qubit rotation gate in a quantum computer performing a lengthy algorithm. However, in the more realistic and currently viable implementations of quantum key distribution this loss due to imperfect recall will turn out to be small compared to the transmission losses

encountered when transmitting single photons through a hundred kilometers of optical fibre. In this case the overall efficiency of the system, considered as a combination of transmission and storage, is therefore decreased only slightly.

4.1 Splitting the memory

The method of breaking the symmetry of the system in a controlled manner investigated in this work is to trigger recall from the two different parts of the memory at two different times. Instead of the original CRIB setup as described in Chapter 3, suppose that the external field controlling the detunings can be manipulated separately in the two spatial segments $A = [0, z_0]$ and $B = (z_0, L]$, where $0 < z_0 < L$.

Assume again that the centre of a temporally localized input pulse propagating in the forward direction arrives at $z = 0$ at time $t = t_p$. The pulse will be absorbed throughout the entire medium from $z = 0$ to $z = L$, as described in Section 3.3.1. Now, instead of reversing the applied detunings and applying a $2kz$ phase shift to the entire memory at time T_0, suppose that recall is triggered from section A at time $T_A > t_p$, and subsequently from section B at time $T_B > T_A$. This situation can be analyzed as follows, by building on the results from the previous chapter.

As in the prior analysis it is assumed that the input pulse, $\Omega_{\mathrm{f}}(0, t)$, is known and that the detunings follow the uniform distribution (3.30). The evolution of the pulse as it travels through the medium is given by (3.34) so that the light field which leaves A, i.e. that portion of the pulse that wasn't absorbed between $z = 0$ and $z = z_0$, is

$$\Omega_{\mathrm{f}}(z_0, t) = \mathrm{e}^{-\alpha z_0/2}\Omega_{\mathrm{f}}(0, t - nz_0/c) \ . \tag{4.1}$$

In Figure 4.1 this corresponds to the portion of the input field that crosses the boundary at $z = z_0$, and is therefore the input pulse to the second segment, B. When the recall from A is performed it behaves as a single memory of length z_0, and the output pulse is

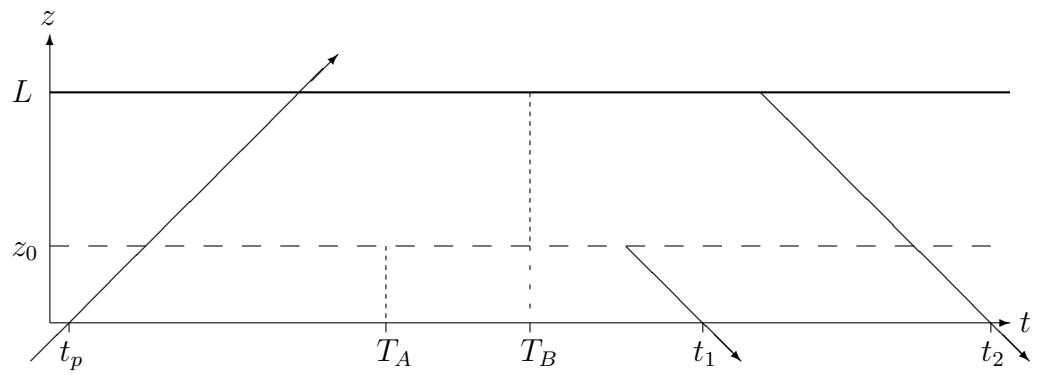

Figure 4.1: Spacetime diagram representing the motion of the pulse peak during the double-recall scheme. The input pulse at $z = 0$ is temporally centred at $t = t_p$; the output pulses, also at $z = 0$ but moving in the backward direction, are temporally centred at t_1 and t_2. The recall time T_A lies at the centre of t_p and t_1, while T_B is at the midpoint of t_p and t_2.

given by

$$\Omega_{\mathrm{b}}^{A}(0,t) = -\mathrm{e}^{-2\Gamma_2(t-T_A)}\frac{1-\mathrm{e}^{-\alpha z_0(1-\eta)}}{1-\eta}\Omega_{\mathrm{f}}(0,-t+2T_A)\ . \tag{4.2}$$

This is the first output from the medium, at time $t = t_1$, as depicted in Figure 4.1. When the segment B is recalled it also acts as a single memory, this one between $z = z_0$ and $z = L$. Its length is therefore $L - z_0$ and its output at $z = z_0$ is

$$\Omega_{\mathrm{b}}^{B}(z_0,t) = -\mathrm{e}^{-2\Gamma_2(t-T_B)}\frac{1-\mathrm{e}^{-\alpha(L-z_0)(1-\eta)}}{1-\eta}\Omega_{\mathrm{f}}(z_0,-t+2T_B)\ .$$

Once again referring to Figure 4.1, this is the field of the second output pulse as it crosses the dashed line at $z = z_0$. Once the pulse has been recalled from B and reached z_0, it no longer shares any coherence with the atoms through which it is propagating. Segment A therefore now acts as it did initially, partially re-absorbing the pulse from B. For $z \in A$ this behaviour of the pulse recalled from B is described by

$$\Omega_{\mathrm{b}}^{B}(z,t) = \mathrm{e}^{-\alpha(z_0-z)/2}\Omega_{\mathrm{b}}^{B}[z_0, t-n(z_0-z)/c]\ . \tag{4.3}$$

The field that exits the medium at $z = 0$ due to the recall in segment B is therefore given

by

$$\Omega_{\rm b}^{B}(0,t) = \mathrm{e}^{-\alpha z_0/2}\Omega_{\rm b}^{B}(z_0, t - nz_0/c) \tag{4.4a}$$

$$= -\mathrm{e}^{-2\Gamma_2(t-nz_0/c-T_B)}\frac{1-\mathrm{e}^{-\alpha(L-z_0)(1-\eta)}}{1-\eta}\mathrm{e}^{-\alpha z_0/2}\Omega_{\rm f}(z_0, -t + nz_0/c + 2T_B) \tag{4.4b}$$

$$= -\mathrm{e}^{-2\Gamma_2(t-nz_0/c-T_B)}\frac{1-\mathrm{e}^{-\alpha(L-z_0)(1-\eta)}}{1-\eta}\mathrm{e}^{-\alpha z_0}\Omega_{\rm f}(0, -t + 2T_B)\ , \tag{4.4c}$$

which corresponds to the final output pulse at $t = t_2$ in Figure 4.1.

The principle of superposition allows the total output from the medium to be written as the sum of $\Omega_{\rm b}^{A}(0,t)$ and $\Omega_{\rm b}^{B}(0,t)$. Before doing so though it is useful to consider an optimization that can be made to minimize the loss that $\Omega_{\rm b}^{B}$ experiences as it travels through segment A.

4.1.1 Optimizing recall efficiency

The pulse recalled from segment B that leaves the medium will be partially re-absorbed as it travels from $z = z_0$ back to $z = 0$, as described by (4.3). Note that the absorption coefficient α depends not only on intrinsic properties of the medium, but is also inversely proportional to γ, the width of the distribution of detunings present. This width in turn depends on the strength of the externally-applied electric field, $\mathbf{E}_{\rm S}$, that creates the Stark shift in the atoms. Therefore, the greater the strength of this electric field the smaller the value of α.

It has already been assumed that the field $\mathbf{E}_{\rm S}$ can be controlled in segments A and B independently. Therefore if the field strength in A is made sufficiently large before the recall of B is initiated, re-absorption effects can be safely neglected. That is, the field recalled from B at a position $z \in A$ can now be written simply as

$$\Omega_{\rm b}^{B}(z,t) = \Omega_{\rm b}^{B}[z_0, t - n(z_0 - z)/c]\ . \tag{4.5}$$

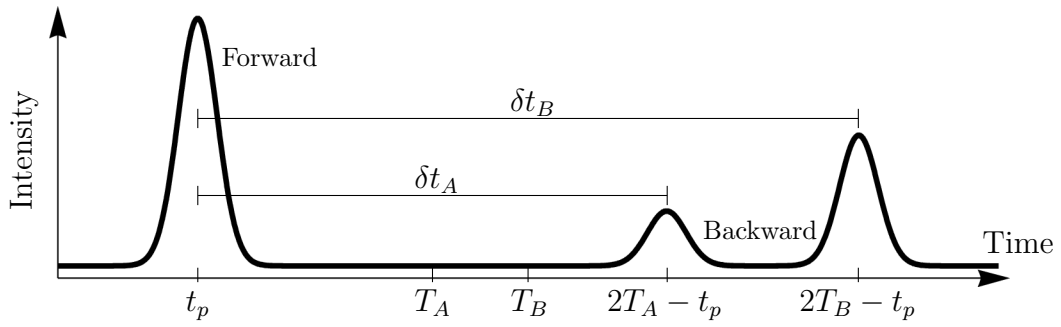

Figure 4.2: A demonstrative plot of the intensity at $z = 0$ during the double recall scheme. The first peak, at $t = t_p$, is the input field. The second and third peaks represent scaled copies of the input pulse reflected about times $t = T_A$ and $t = T_B$, respectively.

Under these considerations then, the net effect is that the recalled pulse is given by

$$\Omega_{\mathrm{b}}^{B}(0,t) = -\mathrm{e}^{-2\Gamma_2(t-nz_0/c-T_B)}\frac{1-\mathrm{e}^{-\alpha(L-z_0)(1-\eta)}}{1-\eta}\mathrm{e}^{-\alpha z_0/2}\Omega_{\mathrm{f}}(0,-t+2T_B)\ . \tag{4.6}$$

4.1.2 The output pulse

The expression for the total output from the memory can now easily be found as the sum of the fields resulting from the two recalls. It is convenient to define a scaling factor for each output pulse. As was the case in Section 3.5, each factor depends on time but can be well-approximated by the value it takes on at the peak of the corresponding pulse. That is,

$$\chi_A := \mathrm{e}^{-2\Gamma_2(T_A-t_p)}\frac{1-\mathrm{e}^{-\alpha z_0(1-\eta)}}{1-\eta} \tag{4.7}$$

and

$$\chi_B := \mathrm{e}^{-2\Gamma_2(T_B-t_p)}\frac{1-\mathrm{e}^{-\alpha(L-z_0)(1-\eta)}}{1-\eta}\ . \tag{4.8}$$

Then, for $t > T_B$,

$$\Omega_{\mathrm{b}}(0,t) = -\chi_A\Omega_{\mathrm{f}}(0,-t+2T_A) - \chi_B\mathrm{e}^{-\alpha z_0/2}\mathrm{e}^{2\Gamma_2 nz_0/c}\Omega_{\mathrm{f}}(0,-t+2T_B)\ . \tag{4.9}$$

From this it is easy to see that two time-reversed copies of the input pulse are re-emitted, with amplitudes that depend on the choice of z_0. The first pulse is a scaled reflection

of the input about the moment of recall T_A. The second pulse is delayed from the first, being reflected about T_B. The storage times of the pulses are defined to be the temporal separation of each of their peaks from the peak of the input pulse, $\delta t_A = 2(T_A - t_p)$ and $\delta t_B = 2(T_B - t_p)$. This is represented in Figure 4.2.

There are two additional factors to note in the term related to the second pulse. The first, $\mathrm{e}^{-\alpha z_0/2}$, is simply the decrease in amplitude due to the electric field passing through segment A, an absorbing medium of length z_0 (cf. Equation [3.34]). The second, $\mathrm{e}^{2\Gamma_2 n z_0/c}$, is slightly more subtle. The scaling factor χ_B contains a term $\mathrm{e}^{-2\Gamma_2(T_B - t_p)}$ that describes the decay of the field due to decoherence effects for the time δt_B. However, since the portion of the pulse that was stored in segment B had to travel the length of segment A twice, a distance $2z_0$, the time spent propagating through A must be subtracted from the storage time. The actual time the pulse spent absorbed is thus $2(T_B - t_p) - 2nz_0/c$, and it is this final term which results in the second exponential in (4.9).

4.1.3 Phase difference

As with the single-recall case each output pulse in this scheme will have a phase difference with respect to the input that depends on its storage time, $\delta\varphi_i = \omega_L \delta t_i$. The phase difference between the two output pulses then depends on the difference in their storage times,

$$\delta\varphi_B - \delta\varphi_A = \omega_L \left(\delta t_B - \delta t_A\right) \ . \tag{4.10}$$

It is useful to express the phase difference modulo 2π. That is, there exists a unique integer m such that

$$\delta\varphi_B - \delta\varphi_A = 2m\pi + \delta\varphi \tag{4.11}$$

and $\delta\varphi \in [0, 2\pi)$. Let this define the physically relevant phase difference $\delta\varphi$ between the two output pulses. Conversely, given a desired phase difference one needs only to time

the recalls appropriately in order to achieve it,

$$\omega_L\left(\delta t_B - \delta t_A\right) = 2m\pi + \delta\varphi \quad \Longrightarrow \quad \delta t_B = \delta t_A + \frac{2m\pi + \delta\varphi}{\omega_L} \ . \tag{4.12}$$

4.2 Recall efficiency

As with the the original CRIB protocol, the percentage of total input energy recalled from the medium is a useful figure of merit for the modified version. Clearly the efficiency of this new protocol will depend on whether the pulse recalled from segment B interacts with segment A on its way through. If it does not then the expression for the output pulse is given by (4.6); otherwise it will be assumed that the absorption coefficient remains unchanged and the output is given by (4.4c). The only difference between these two expressions is a factor of $\mathrm{e}^{-\alpha z_0/2}$, so they can both be expressed as

$$\Omega_{\mathrm{b}}^{B}(0,t) = -\mathrm{e}^{-2\Gamma_2(t-nz_0/c-T_B)}\frac{1-\mathrm{e}^{-\alpha(L-z_0)(1-\eta)}}{1-\eta}\mathrm{e}^{-\alpha z_0 q}\Omega_{\mathrm{f}}(0,-t+2T_B) \ , \tag{4.13}$$

where $q \in \{1, 1/2\}$ describes whether or not re-absorption occurs. Of course, q could take on other values if the absorption coefficient of segment A was altered during recall, but not taken arbitrarily close to zero. However, there is no reason to increase the coefficient so examining these two cases will place bounds on the expected recall efficiency.

The definitions used in Chapter 3 are still of use, but the output energy must be re-examined for this new case,

$$E_{\mathrm{b}} = \int_{T_A}^{\infty} \mathrm{d}t \ \left|\Omega_{\mathrm{b}}(0,t)\right|^2 \tag{4.14a}$$

$$= \int_{T_A}^{\infty} \mathrm{d}t \ \left|\chi_A\Omega_{\mathrm{f}}(0,-t+2T_A) + \chi_B\mathrm{e}^{-\alpha z_0 q}\mathrm{e}^{2\Gamma_2 nz_0/c}\Omega_{\mathrm{f}}(0,-t+2T_B)\right|^2 \tag{4.14b}$$

$$\begin{aligned} = \chi_A^2\int_{T_A}^{\infty} \mathrm{d}t \ \left|\Omega_{\mathrm{f}}(0,-t+2T_A)\right|^2 + \chi_B^2\mathrm{e}^{-2\alpha z_0 q}\mathrm{e}^{4\Gamma_2 nz_0/c}\int_{T_A}^{\infty} \mathrm{d}t \ \left|\Omega_{\mathrm{f}}(0,-t+2T_B)\right|^2 \\ + \chi_A\chi_B\mathrm{e}^{-\alpha z_0 q}\mathrm{e}^{2\Gamma_2 nz_0/c}\left(\int_{T_A}^{\infty} \mathrm{d}t\,\Omega_{\mathrm{f}}(0,-t+2T_A)\Omega_{\mathrm{f}}^{*}(0,-t+2T_B) + \mathrm{c.c.}\right). \end{aligned} \tag{4.14c}$$

The first two integrals are straight-forward to deal with, as will be done soon. The third integral is worth investigating first however. Note that by defining the variable $s = -t + 2T_A$ the integral can be rewritten as

$$\mathcal{C}[2(T_A - T_B)] := \int_{-\infty}^{T_A} \mathrm{d}s\, \Omega_{\mathrm{f}}(0,s)\Omega_{\mathrm{f}}^*[0, s - 2(T_A - T_B)] \ . \tag{4.15}$$

Since by assumption $\Omega_{\mathrm{f}}(0,s)$ vanishes for all $s > T_A$ the upper limit can be extended to infinity without affecting the value of the integral. It is then seen that $\mathcal{C}$ is the autocorrelation of Ω_{f} at $z = 0$. Its value depends explicitly on the duration between the recalls performed on the two sections A and B. For arbitrary T_A and T_B this obviously cannot be evaluated further without knowledge of the specific form of $\Omega_{\mathrm{f}}(0,t)$. In the case of interest here though it is assumed that the output pulses are sufficiently far apart to reasonably define two time bins (as depicted in Figure 4.2). That is, the time between the pulses is large compared to their widths. In this case, with no further assumptions on the form of $\Omega_{\mathrm{f}}(0,t)$, it is clear that $\mathcal{C} = 0$ since there is no moment in time at which the integrand is non-negligible.

With this knowledge about the third term in the expression for the recalled energy, and with appropriate changes to the variables of integration, E_{b} simplifies to

$$E_{\mathrm{b}} = \chi_A^2 \int_{-\infty}^{T_A} \mathrm{d}t\ |\Omega_{\mathrm{f}}(0,t)|^2 + \chi_B^2 \mathrm{e}^{-2\alpha z_0 q} \mathrm{e}^{4\Gamma_2 n z_0/c} \int_{-\infty}^{T_B} \mathrm{d}t\ |\Omega_{\mathrm{f}}(0,t)|^2 \ . \tag{4.16}$$

Since $\Omega_{\mathrm{f}}(0,t)$ is assumed to vanish at every time between T_A and T_B, the upper limit of the second integral can be reduced to T_A so that the total recalled energy can be written in terms of the input energy (3.56) as,

$$E_{\mathrm{b}} = \left(\chi_A^2 + \chi_B^2 \mathrm{e}^{-2\alpha z_0 q} \mathrm{e}^{4\Gamma_2 n z_0/c}\right) E_{\mathrm{f}} \ . \tag{4.17}$$

4.2.1 Dependence on z_0

The output of this new protocol for generating two smaller pulses from a single larger one is really a function of z_0, the position at which the medium is 'split'. The efficiency

of the transformation, equivalent to how much of the input energy is in the output, is found from (4.17). Using the definitions (4.7) and (4.8) of χ_A and χ_B the efficiency is

$$\mu(z_0) := \mathrm{e}^{-4\Gamma_2(T_A-t_p)}\left(\frac{1-\mathrm{e}^{-\alpha z_0(1-\eta)}}{1-\eta}\right)^2 + \mathrm{e}^{-2\alpha z_0 q}\mathrm{e}^{-4\Gamma_2(T_B-t_p-nz_0/c)}\left(\frac{1-\mathrm{e}^{-\alpha(L-z_0)(1-\eta)}}{1-\eta}\right)^2 . \tag{4.18}$$

The value of z_0 can range over the full length of the medium, from 0 to L. The limiting cases are therefore

$$\mu(0) = \mathrm{e}^{-4\Gamma_2(T_B-t_p)}\left(\frac{1-\mathrm{e}^{-\alpha L(1-\eta)}}{1-\eta}\right)^2 = \chi^2\big|_{T_0=T_B} \tag{4.19}$$

and

$$\mu(L) = \mathrm{e}^{-4\Gamma_2(T_A-t_p)}\left(\frac{1-\mathrm{e}^{-\alpha L(1-\eta)}}{1-\eta}\right)^2 = \chi^2\big|_{T_0=T_A} \ . \tag{4.20}$$

These results agree exactly with what should be expected for them based on the efficiency of the single-recall scheme, (3.60). Setting $z_0 = 0$ means that segment B comprises the entire medium, which then behaves as a single-recall memory with recall triggered at time T_B. Similarly $z_0 = L$ implies that the whole medium is segment A, so the single-recall result for triggering at $t = T_A$ is recovered.

4.2.2 The ideal case

It has been seen that the effect of a non-zero decay rate is to decrease the amplitude of the output pulse with increased storage time, and thus to decrease the recall efficiency. However Γ_2 has essentially no impact on the shape of the output pulse. Therefore the ideal case of $\Gamma_2 = 0$ will be investigated, though it should be kept in mind that any values obtained for efficiency or amplitude are merely upper bounds on the physical situation.

In this case the results of the previous subsection simplify significantly. The scaling coefficients become $\chi_A = 1 - \mathrm{e}^{-\alpha z_0}$ and $\chi_B = 1 - \mathrm{e}^{-\alpha(L-z_0)}$, and the output pulse is given

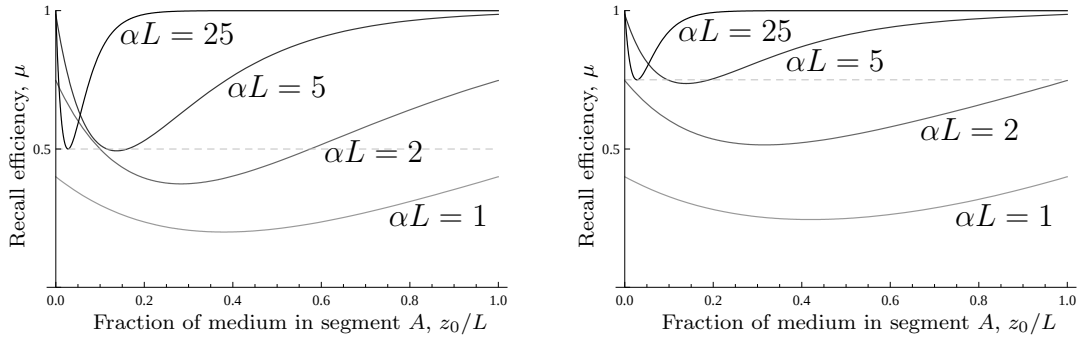

(a) Re-absorption in A, $q = 1$

(b) No re-absorption in A, $q = 1/2$

Figure 4.3: The dependence of recall efficiency on the fraction of the memory recalled as segment A. The point $z_0/L = 0$ corresponds to the entire medium being recalled as segment B, whereas $z_0/L = 1$ means that segment A is the whole memory. Various optical depths αL are shown. Each curve has a unique minimum, μ_m, which increases with αL; the theoretical maximum for μ_m is 0.5 when $q = 1$ and is 0.75 when $q = 1/2$. In either case the limit is attained when $\alpha L \to \infty$. Note though that even $\alpha L = 5$ comes very close to the limit in both cases.

by, for $t > T_B$,

$$\Omega_\mathrm{b}(0,t) = -\left(1-\mathrm{e}^{-\alpha z_0}\right)\Omega_\mathrm{f}(0,-t+2T_A) - \left(1-\mathrm{e}^{-\alpha(L-z_0)}\right)\mathrm{e}^{-\alpha z_0 q}\Omega_\mathrm{f}(0,-t+2T_B)\ . \quad (4.21)$$

The ideal recall efficiency for a medium of finite length is given by

$$\mu(z_0)|_{\Gamma_2=0} = \left(1-\mathrm{e}^{-\alpha z_0}\right)^2 + \left(1-\mathrm{e}^{-\alpha(L-z_0)}\right)^2 \mathrm{e}^{-2\alpha z_0 q}\ . \quad (4.22)$$

As before, taking z_0 to either 0 or L recovers the single-recall result. It is now possible to determine the behaviour of the efficiency as a function of z_0/L, the fraction of the medium that comprises segment A. Figure 4.3 shows this behaviour for both cases, with and without re-absorption in A. As can be seen, the largest efficiency for a given optical depth is always when the memory is recalled as a whole, using the original CRIB protocol. When the memory is split under the new protocol, there exists a unique minimum value for the efficiency.

It is frequently physically reasonable to assume that the optical depth of the medium

as a whole is sufficiently large that the term $\mathrm{e}^{-\alpha L}$ can be neglected. This further simplifies the recall efficiency, yielding

$$\mu(z_0) = \left(1 - \mathrm{e}^{-\alpha z_0}\right)^2 + \mathrm{e}^{-2\alpha z_0 q} \ . \tag{4.23}$$

It turns out that the position which minimizes this function is the same for both $q = 1$ and $q = 1/2$; this position is $z_\mathrm{m} = \alpha^{-1} \ln 2$.

Re-absorption, $q = 1$

When the absorption coefficient of segment A remains constant throughout the protocol so that the pulse recalled from segment B experiences absorption as it passes through A, the ideal efficiency (4.22) becomes

$$\mu = \left(1 - \mathrm{e}^{-\alpha z_0}\right)^2 + \mathrm{e}^{-2\alpha z_0} \ . \tag{4.24}$$

When the memory is split at z_m the efficiency is $\mu_\mathrm{m} = 1/2$, and the output pulse is given by

$$-\frac{1}{2}\left[\Omega_\mathrm{f}(0, -t + 2T_A) + \Omega_\mathrm{f}(0, -t + 2T_B)\right] \ . \tag{4.25}$$

The minimum efficiency corresponds to the case of equal-amplitude pulses being recalled from the memory.

No re-absorption, $q = 1/2$

Similar analysis when the atoms of segment A are caused to not re-absorb the pulse from B results in an ideal efficiency of

$$\mu = \left(1 - \mathrm{e}^{-\alpha z_0}\right)^2 + \mathrm{e}^{-\alpha z_0} \ . \tag{4.26}$$

In this case the minimum efficiency is greater; when split at z_m the recall efficiency is $\mu_\mathrm{m} = 3/4$. The amplitude of the pulse recalled from A remains the same, but as expected the amplitude of the pulse due to B increases; the output pulse is

$$-\frac{1}{2}\Omega_\mathrm{f}(0, -t + 2T_A) - \frac{1}{\sqrt{2}}\Omega_\mathrm{f}(0, -t + 2T_B) \ . \tag{4.27}$$

In this case, obtaining equal-amplitude output pulses requires splitting the medium at

$$z_0 = \frac{2}{\alpha}\text{arcsinh}\left(\frac{1}{2}\right) \ . \tag{4.28}$$

Since this position is not at z_m, the output efficiency is slightly higher in this case, $\mu = 3 - \sqrt{5} \approx 0.764$.

4.3 Manipulating qubits

The most commonly used photonic degree of freedom employed to encode information in photonic qubits propagating through optical fibres is that of arrival time. Polarization is generally regarded to be the most intuitive choice, and is frequently used to introduce quantum key distribution via the BB84 protocol. However, standard telecommunications fibres do not preserve the state of polarization of light propagating through them. This is why so-called time-bin qubits are a better choice than polarization qubits in most implementations of quantum key distribution.

4.3.1 Time-bin qubits

The concept of time-bin qubits was introduced in Section 1.3; they will be further motivated and explored here. By definition the state space of a qubit is two-dimensional. Therefore any physical system in which one plans to encode a qubit must have a Hilbert space containing a two-dimensional subspace. If two optical pulses travel sequentially through air or through an optical fibre, any variations in the index of refraction will affect both equally. Therefore the time separating the two pulse peaks will remain constant during transmission. This is the motivation behind the definition of time-bin qubits.

Consider a detector that records the time at which a photon is detected. One can define an arbitrary time as the separation between two states – either the photon arrives before that time and is 'early', or arrives after that time and is 'late'. Of course, to

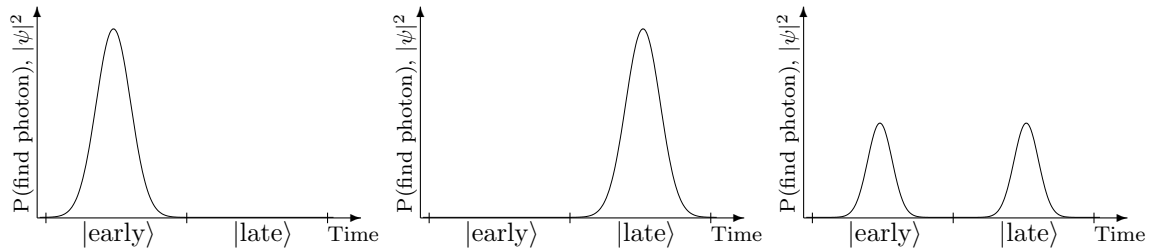

(a) Temporal probability distribution for a photon in the state $|\text{early}\rangle$

(b) A photon in the state $|\text{late}\rangle$

(c) A superposition state such as $\frac{1}{\sqrt{2}}(|\text{early}\rangle + |\text{late}\rangle)$

Figure 4.4: Graphical representation of photons in three different time-bin states. (a) The state $|\text{early}\rangle$, in which the photon has essentially unit probability of arriving at a detector during the first time bin. (b) When the photon will arrive in the second time bin it is in the state $|\text{late}\rangle$. (c) A photon prepared in a superposition of $|\text{early}\rangle$ and $|\text{late}\rangle$ has some non-negligible probability to arrive during either time bin; in this graphic there is equal probability for both.

be useful for encoding more than a single qubit a window during which the photon is expected to arrive should be defined, allowing multiple sequential photons to encode multiple bits. That is, let T be the width of such a window, or bin, and define that if a photon arrives between $t = -T$ and $t = 0$ then it is in the state $|\text{early}\rangle$; arrival between $t = 0$ and $t = T$ corresponds to the state $|\text{late}\rangle$. This system now repeats: For $m \in \mathbb{Z}$, a photon arriving between $t = 2(m-1)T$ and $2mT$ is $|\text{early}\rangle$; one arriving between $t = 2mT$ and $t = 2(m+1)T$ is $|\text{late}\rangle$.

4.3.2 State creation

Under this definition, all photons impinging on the detector must be measured to be in exactly one of $|\text{early}\rangle$ and $|\text{late}\rangle$, assuming either perfect detection efficiency or post-selection of detection events. Under the further assumption that the photons are known to have been prepared in states such that there is negligible probability for them to arrive outside of these two detection windows, this defines a two-dimensional state space for the photons. To be of practical use one must of course define the time-bin width T to be longer than the temporal duration of the photonic pulses that will be used.

It may already be clear that given an input photon in a single well-defined time bin, the double-recall CRIB protocol allows one to transform the photon into an arbitrary superposition of $|\text{early}\rangle$ and $|\text{late}\rangle$, making the memory device able to act like a variable beam splitter and phase shifter. This will now be shown explicitly. For simplicity the ideal case, with $\Gamma_2 = 0$, $\alpha L \to \infty$, and $q = 1/2$, will be assumed for the remainder of this chapter. Define

$$|0\rangle := |\text{early}\rangle \qquad \text{and} \qquad |1\rangle := |\text{late}\rangle \ , \tag{4.29}$$

and let the desired output state be given by

$$a|0\rangle + b\mathrm{e}^{\mathrm{i}\varphi}|1\rangle \tag{4.30}$$

with $a, b, \varphi \in \mathbb{R}$ and $a^2 + b^2 = 1$. Note that these states define a so-called computational basis, and that the state $|1\rangle$ defined here is unrelated to the atomic energy state employed in Chapter 2. The two are not used in the same context, so no confusion should arise from this duplicate definition of the state $|1\rangle$. It is also useful at this point to define a pair of conjugate bases,

$$\mathcal{B}_0 := \{|0\rangle, |1\rangle\} \ , \qquad \text{and} \qquad \mathcal{B}_+ := \{|+\rangle, |-\rangle\} \ , \tag{4.31}$$

where the states in $\mathcal{B}_+$ are defined by

$$|+\rangle := \frac{|0\rangle + |1\rangle}{\sqrt{2}} \ , \quad |-\rangle := \frac{|0\rangle - |1\rangle}{\sqrt{2}} \ . \tag{4.32}$$

In order to prepare the state (4.30), one has only to determine the value of z_0 that will produce the amplitude coefficients a and b. The phase φ is determined simply by adding an appropriate delay to T_B, as described in Subsection 4.1.3. Note that this delay is orders of magnitude shorter than the width of a time bin, so that the shift will not affect the magnitude of a or b.

The normalized recalled state is

$$-\frac{(1 - \mathrm{e}^{-\alpha z_0})\,|0\rangle + \mathrm{e}^{-\alpha z_0/2}|1\rangle}{\sqrt{1 - \mathrm{e}^{-\alpha z_0} + \mathrm{e}^{-2\alpha z_0}}} \tag{4.33}$$

from which the coefficients a and b can be read off. Either can be used to determine the appropriate value of z_0. For example,

$$b = -\frac{\mathrm{e}^{-\alpha z_0/2}}{\sqrt{1-\mathrm{e}^{-\alpha z_0}+\mathrm{e}^{-2\alpha z_0}}} \qquad \Longrightarrow \qquad z_0 = \frac{1}{\alpha}\mathrm{arccosh}\left(\frac{1+b^2}{2b^2}\right) . \tag{4.34}$$

In particular, a qubit initially in the state $|1\rangle$ can be transformed into the state $|+\rangle$ by setting $b = 1/\sqrt{2}$. One would also set $b = 1/\sqrt{2}$ to obtain an output of $|-\rangle$, but at the same time would adjust the phase between the peaks of the two ouput pulses as described in Subsection 4.1.3.

From these results it is straightforward to see how the effects of either or both of a beam splitter and a phase shifter can be reproduced from a double-recall CRIB device. In fact, it is the combination of these two things which can create the state (4.30).

Chapter 5

Simulations

The results of the preceding analysis can be supported by numerical integration of the equations of motion for the system, either in the low-excitation form involving the polarization σ or in the more general setting provided by the Bloch equations (2.14). Programatically the difference between the two situations is rather minor, so both sets of equations have been simulated as part of this body of work. The primary purpose of the simulations is pedagogical, through the pictures they are able to produce of the evolution of the system within the medium. They also provide the opportunity to investigate distributions of atomic detunings that are more general than those that fall under the assumptions of the previous chapters. These simulations were written in MATLAB [Mat07] and the source code for the `.m` file can be found in Appendix A. Based on the strong similarities between the two sets of code, it was deemed sufficient to include only the one that simulates σ. This is also the version which was used to generate the majority of the graphics in this chapter. The results of simulating the different sets of equations are essentially identical in the case of light pulses equivalent to a few photons in terms of energy. For example, consider the evolution of the fields presented in Figure 5.1.

In order to facilitate comparisons with and use of experimental data the simulations make us of SI units. Except where otherwise specified, the values used to create the results in this chapter were those stated in Table 5.1. The simulations, and indeed the Maxwell-Bloch equations, determine the evolution of a classical electric field. One can still make use of them to analyze the single-photon case though; due to the linearity of the equations of motion, the fields Ω_{f} and Ω_{b} can be interpreted either as classical electric fields or as the probability amplitudes for a photonic state.

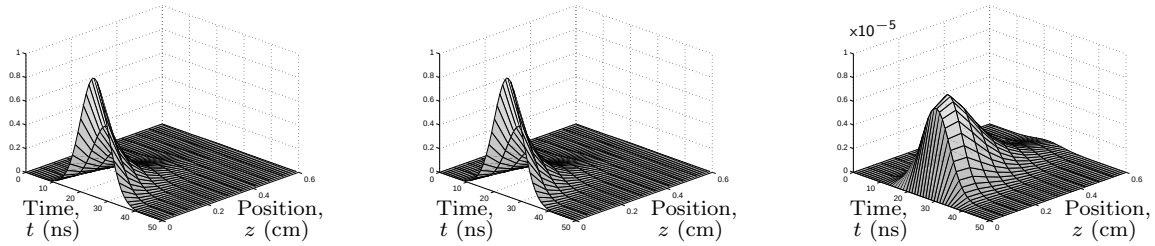

(a) Simulating the absorption of a single photon based on the full Maxell-Bloch equations, (5.6)

(b) Simulating the same initial conditions using the simplified Maxwell-Bloch equations, (5.5)

(c) Absolute difference between the two simulation results

Figure 5.1: A comparison of simulation results arising from different forms of the Maxwell-Bloch equations. Note that the vertical scale on the difference plot (c) is five orders of magnitude smaller than the scales of the simulation results (a) and (b). It is clear that there is no disadvantage to using the simpler form found in (5.5).

To determine the classical electric field amplitude corresponding to a single photon the classical and quantum energies may be equated. For the classical case assume that the pulse is Gaussian in all three spatial dimensions, and has cylindrical symmetry about the direction of propagation. Let the cross-sectional width of the pulse be given by w; its width in the z direction is $c\,\delta t$. This results in

$$\mathbf{E}(z) = \boldsymbol{\varepsilon} E_0 \mathrm{e}^{-\mathrm{i}(\omega_L t - kz)} \exp\left(\frac{-\left(x^2+y^2\right)}{w^2}\right) \exp\left(\frac{-z^2}{c^2\delta t^2}\right) + \text{c.c.} \tag{5.1}$$

The task now is to determine the value of E_0 in terms of the other known constants involved. The corresponding magnetic field has magnitude $|\mathbf{B}| = |\mathbf{E}|/c$, resulting in the linear energy density being given by

$$u(z) = \frac{\epsilon_0}{2} \int_{-\infty}^{\infty} \mathrm{d}x\,\mathrm{d}y\, \left(|\mathbf{E}|^2 + c^2|\mathbf{B}|^2\right) = \epsilon_0 \int_{-\infty}^{\infty} \mathrm{d}x\,\mathrm{d}y\,|\mathbf{E}|^2 \ . \tag{5.2}$$

The Gaussian integral over the transverse directions simply evaluates to πw^2. The total energy stored in the field is therefore

$$U = \int_{-\infty}^{\infty} \mathrm{d}z\, u(z) = \epsilon_0 E_0^2 \pi w^2 \int_{-\infty}^{\infty} \mathrm{d}z\, \mathrm{e}^{-2z^2/c^2\delta t^2} = \epsilon_0 E_0^2 w^2 c\,\delta t \sqrt{\frac{\pi^3}{2}} \ . \tag{5.3}$$

It is this energy which is equated with the quantum-mechanical expression for the energy

Parameter	MATLAB name	Numeric value	Comments
Simulation duration	`tDuration`	300×10^{-9}	300 ns
Length of medium	`L`	0.006	6 mm
Central frequency, ω_L	`wL`	4.77×10^{13}	47.7 THz or 1000 nm
Temporal pulse width	`tau`	10×10^{-9}	10 ns
Input pulse centre, t_p	`tp`	25×10^{-9}	25 ns
Time to recall A, T_A	`TA`	100×10^{-9}	100 ns
Time to recall B, T_B	`TB`	125×10^{-9}	125 ns
Bandwidth of medium	`gam`	10^9	1 GHz
Dopant-ion density, N	`ionDens`	10^{25}	10^{19} cm^{-3}
Dipole moment, $\wp$	`p`	1.67×10^{-32}	Erbium in silicate glass
Decoherence rate, Γ_2	`Gam2`	0	The ideal case
Refractive index, n	`nr`	1.5	glass
Beam width, w	`beamWidth`	4×10^{-3}	4 mm
Speed of light, c	`c`	299792458	m/s
Planck's contant, $\hbar$	`hb`	1.05457×10^{-34}	J s
Electric constant, ϵ_0	`ep0`	8.854×10^{-12}	C m
Magnetic constant, μ_0	`mu0`	$4\pi \times 10^{-7}$	N/A^2

Table 5.1: Names and values of physical parameters as they appear in the MATLAB simulation code.

of a photon, $U = \hbar\omega_L$. Doing so leads to a solution for the electric field amplitude,

$$E_0 = \sqrt{\frac{\sqrt{2}\hbar\omega_L}{\pi^{3/2} w^2 \epsilon_0 c\, \delta t}} \ . \tag{5.4}$$

This value is calculated by the simulation, based on user-programmable values for the laser frequency, pulse duration, and beam width.

5.1 Forward-propagating Maxwell-Bloch simulation

5.1.1 Co-moving frame

The simulations numerically integrate one of two forms of the Maxwell-Bloch equations. One of these makes use of σ in the low-excitation limit,

$$\left(\frac{n}{c}\partial_t + \partial_z\right)\Omega_{\mathrm{f}}(z,t) = \mathrm{i}\beta\int_{-\infty}^{\infty}\mathrm{d}\Delta\, g(\Delta)\sigma_{\mathrm{f}}(z,t,\Delta)\ , \tag{5.5a}$$

$$\partial_t\sigma_{\mathrm{f}}(z,t,\Delta) = (\mathrm{i}\Delta - \Gamma_2)\sigma_{\mathrm{f}}(z,t,\Delta) + \mathrm{i}\Omega_{\mathrm{f}}(z,t)\ , \tag{5.5b}$$

along with the corresponding equations for the backward-moving pulse. The other is their full form, with decay terms added, given by

$$\left(\frac{n}{c}\partial_t + \partial_z\right)\Omega_{\mathrm{f}}(z,t) = \mathrm{i}\beta\int_{-\infty}^{\infty}\mathrm{d}\Delta\, g(\Delta)\left[r_1'(z,t,\Delta) - \mathrm{i}r_2'(z,t,\Delta)\right]\ , \tag{5.6a}$$

$$\partial_t r_1'(z,t,\Delta) = \Delta r_2'(z,t,\Delta) - \Gamma_2 r_1'\ , \tag{5.6b}$$

$$\partial_t r_2'(z,t,\Delta) = -\Delta r_1'(z,t,\Delta) + \Omega_{\mathrm{f}}(z,t) r_3'(z,t,\Delta) - \Gamma_2 r_2'\ , \tag{5.6c}$$

$$\partial_t r_3'(z,t,\Delta) = -\Omega_{\mathrm{f}}(z,t) r_2'(z,t,\Delta) - \Gamma_1(1 + r_3')\ , \tag{5.6d}$$

as well as the equivalent forms for a pulse propagating in the negative z direction. Here $\Gamma_1 = 1/T_1$ is the inverse of the natural lifetime of the excited state. The combination of the two forms results in four sets of coupled differential equations, comprised of a total of four PDEs and eight ODEs.

A coordinate transformation to a frame moving at the speed of light in the medium allows the four PDEs ([5.6a], [5.5a], and their backward-moving counterparts) to be recast as ODEs, without affecting the form of the other eight equations. This procedure is the same for all four sets of equations, so it suffices to describe the process in detail for one of them. Specifically, consider (5.5a).

The first step is to define a new set of coordinates, $\xi = z$ and $\tau = t - nz/c$. The

paraxial wave operator transforms to this new reference frame as

$$\frac{n}{c}\partial_t + \partial_z = \frac{n}{c}\left(\frac{\partial\xi}{\partial t}\partial_\xi + \frac{\partial\tau}{\partial t}\partial_\tau\right) + \left(\frac{\partial\xi}{\partial z}\partial_\xi + \frac{\partial\tau}{\partial z}\partial_\tau\right) = \frac{n}{c}\partial_\tau + \partial_\xi - \frac{n}{c}\partial_\tau = \partial_\xi \ , \tag{5.7}$$

while the partial derivative with respect to time simply becomes

$$\partial_t = \partial_\tau \ . \tag{5.8}$$

With the definitions $\bar{\Omega}_\mathrm{f}(\xi,\tau) := \Omega_\mathrm{f}(z,t)$ and $\bar{\sigma}_\mathrm{f}(\xi,\tau,\Delta) := \sigma_\mathrm{f}(z,t,\Delta)$, the equations (5.5) transform as

$$\partial_\xi\bar{\Omega}_\mathrm{f}(\xi,\tau) = \mathrm{i}\beta\int_{-\infty}^{\infty}\mathrm{d}\Delta\, g(\Delta)\bar{\sigma}_\mathrm{f}(\xi,\tau,\Delta) \ , \tag{5.9a}$$

$$\partial_\tau\bar{\sigma}_\mathrm{f}(\xi,\tau,\Delta) = (\mathrm{i}\Delta - \Gamma_2)\bar{\sigma}_\mathrm{f}(\xi,\tau,\Delta) + \mathrm{i}\bar{\Omega}_\mathrm{f}(\xi,\tau) \ . \tag{5.9b}$$

Given a condition for the initial state of the atoms at some time τ_0, $\bar{\sigma}_\mathrm{f}(\xi,\tau_0,\Delta)$, and a boundary condition for the light field over all times at a spatial position ξ_0, $\bar{\Omega}_\mathrm{f}(\xi_0,\tau)$, the evolution equation (5.9b) can be solved for the behaviour of the atoms at position ξ_0 for all time, $\bar{\sigma}_\mathrm{f}(\xi_0,\tau,\Delta)$. This in turn allows the right-hand side of (5.9a) to be evaluated at ξ_0; now with both $\bar{\Omega}_\mathrm{f}(\xi_0,\tau)$ and $\partial_\xi\bar{\Omega}_\mathrm{f}(\xi_0,\tau)$ known, an approximation of $\bar{\Omega}_\mathrm{f}(\xi_1,\tau)$ can be made, where $\xi_1 = \xi_0 + \delta\xi$ represents a position one 'step' forward into the medium. This process can now be repeated to solve for $\bar{\sigma}_\mathrm{f}(\xi_1,\tau,\Delta)$ and subsequently $\bar{\Omega}_\mathrm{f}(\xi_2,\tau)$, and so on. In this manner the evolution of the pulse through the medium can be solved over a given duration and length. A visual depiction of this process can be found in Figure 5.2.

In the case of interest here, the initial condition for the atomic polarization is given by $\bar{\sigma}_\mathrm{f}(\xi,\tau_0,\Delta) = 0$, since initially all atoms in the medium are in the ground state. The boundary condition for the light field at $\xi = \xi_0$ represents the pulse entering the medium that is to be stored.

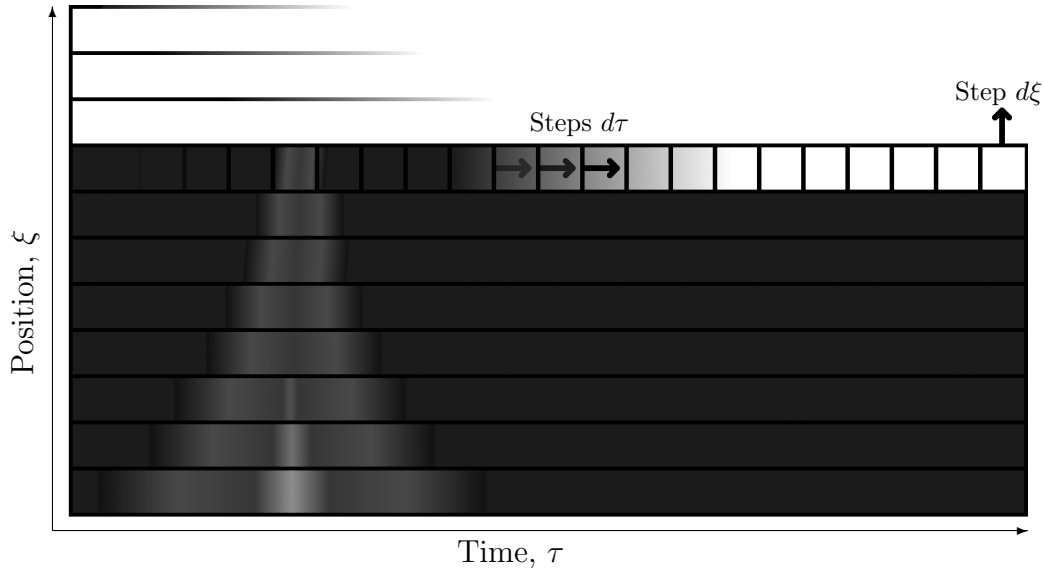

Figure 5.2: Schematic representation of the simulation grid. The atomic polarization $\bar{\sigma}_{\mathrm{f}}$ is evolved in steps from its initial value at the left to its final value at the right for the lowest horizontal slice. These values are then used to propagate the field $\bar{\Omega}_{\mathrm{f}}$ up to the next slice, and the process repeats.

5.1.2 Runge-Kutta algorithm

The method chosen to solve (5.9b) for the temporal evolution of the atoms is the well-known fourth-order Runge-Kutta algorithm, commonly referred to as RK4 (see for example [WA04]). This method allows an ODE of the form

$$\partial_\tau \bar{\sigma}_{\mathrm{f}}(\xi, \tau, \Delta) = f\left(\tau, \bar{\sigma}_{\mathrm{f}}\right) \tag{5.10}$$

to be solved for a given ξ and Δ at a finite set of times, $\{\tau_j\}$, with uniform spacing $\delta\tau = \tau_{j+1} - \tau_j$. For each fixed Δ and ξ, (5.9b) is of this form with

$$f\left(\tau, \bar{\sigma}_{\mathrm{f}}\right) := (\mathrm{i}\Delta - \Gamma_2)\bar{\sigma}_{\mathrm{f}} + \mathrm{i}\bar{\Omega}_{\mathrm{f}} \tag{5.11}$$

If the value of $\bar{\sigma}_\mathrm{f}$ is known at time τ_j, then its value at the next time, τ_{j+1}, can be found as follows. First, four coefficients are calculated via

$$a_1 = \delta\tau \left[(\mathrm{i}\Delta - \Gamma_2)\bar{\sigma}_\mathrm{f}(\xi, \tau_j, \Delta) + \mathrm{i}\bar{\Omega}_\mathrm{f}(\xi, \tau_j)\right] \ , \tag{5.12a}$$

$$a_2 = \delta\tau \left[(\mathrm{i}\Delta - \Gamma_2)\left(\bar{\sigma}_\mathrm{f}(\xi, \tau_j, \Delta) + \frac{a_1}{2}\right) + \mathrm{i}\bar{\Omega}_\mathrm{f}(\xi, \tau_{j+1/2})\right] \ , \tag{5.12b}$$

$$a_3 = \delta\tau \left[(\mathrm{i}\Delta - \Gamma_2)\left(\bar{\sigma}_\mathrm{f}(\xi, \tau_j, \Delta) + \frac{a_2}{2}\right) + \mathrm{i}\bar{\Omega}_\mathrm{f}(\xi, \tau_{j+1/2})\right] \ , \tag{5.12c}$$

$$a_4 = \delta\tau \left[(\mathrm{i}\Delta - \Gamma_2)\left(\bar{\sigma}_\mathrm{f}(\xi, \tau_j, \Delta) + a_3\right) + \mathrm{i}\bar{\Omega}_\mathrm{f}(\xi, \tau_{j+1})\right] \ , \tag{5.12d}$$

and then $\bar{\sigma}_\mathrm{f}$ is calculated at the next time step as

$$\bar{\sigma}_\mathrm{f}(\xi, \tau_{j+1}, \Delta) = \bar{\sigma}_\mathrm{f}(\xi, \tau_j, \Delta) + \frac{a_1 + 2a_2 + 2a_3 + a_4}{6} \ . \tag{5.13}$$

It is assumed that the functional dependence of the input pulse on the time variable τ is known at the start of the medium, $\xi = \xi_0$. However, in general during the simulation the values of $\bar{\Omega}_\mathrm{f}$ will only be known at the discrete times $\{\tau_j\}$. This poses a problem in determining a_2 and a_3, which depend on the value of $\bar{\Omega}_\mathrm{f}$ mid-way between two such times. As long as $\delta\tau$ is sufficiently small and the input pulse is slowly-varying, as has been assumed since Section 2.3, this mid-point value can be adequately approximated by a linear interpolation,

$$\bar{\Omega}_\mathrm{f}(\xi, \tau_{j+1/2}) = \frac{\bar{\Omega}_\mathrm{f}(\xi, \tau_j) + \bar{\Omega}_\mathrm{f}(\xi, \tau_{j+1})}{2} \ . \tag{5.14}$$

In order to be prepared for the integral over Δ in (5.9a) an array of polarizations is created, indexed by the detuning Δ and covering the support of $g(\Delta)$, which is also specified at a discrete set of detunings $\{\Delta_k\}$. The above algorithm is used to evolve each of these polarizations $\bar{\sigma}_\mathrm{f}(\xi, \tau_j, \Delta_k)$.

5.1.3 Finite difference method

As with the time and detuning domains, the length of the medium is discretized into a set of points $\{\xi_i\}$. The desired input pulse is then specified as $\bar{\Omega}_\mathrm{f}(\xi_0, \tau_j)$ for each j in the

simulation's time window. After the atomic polarization has been found for each time at position ξ_i, the value of this integral is approximated for each τ_j by

$$\int_{-\infty}^{\infty} \mathrm{d}\Delta\, g(\Delta)\bar{\sigma}_\mathrm{f}(\xi_i,\tau_j,\Delta) \approx \sum_k \delta\Delta\, g(\Delta_k)\bar{\sigma}_\mathrm{f}(\xi_i,\tau_j,\Delta_k) =: \delta\Omega(\xi_i,\tau_j)\ , \tag{5.15}$$

where $\delta\Delta$ is the uniform spacing between detunings. Since there is no good method of approximating $\bar{\sigma}_\mathrm{f}$ at $\xi_{i+1/2}$ and ξ_{i+1} until $\bar{\Omega}_\mathrm{f}$ is known at those positions, the RK4 algorithm cannot be used again here.

However, as mentioned at the end of the previous section the pulse envelope $\bar{\Omega}_\mathrm{f}$ is assumed to be slowly-varying, in both time and space, so a simpler method of propagating it to the next position is acceptable. The spatial derivative in (5.9a) is approximated using the finite difference method, i.e. Newton's quotient

$$\partial_\xi \bar{\Omega}_\mathrm{f}(\xi_i,\tau_j) \approx \frac{\bar{\Omega}_\mathrm{f}(\xi_{i+1},\tau_j) - \bar{\Omega}_\mathrm{f}(\xi_i,\tau_j)}{\delta\xi}\ . \tag{5.16}$$

Equating this to $\mathrm{i}\beta$ times (5.15) allows the value of the pulse at the next position to be determined,

$$\bar{\Omega}_\mathrm{f}(\xi_{i+1},\tau_j) = \bar{\Omega}_\mathrm{f}(\xi_i,\tau_j) + \mathrm{i}\beta\,\delta\xi\,\delta\Omega(\xi_i,\tau_j)\ . \tag{5.17}$$

5.1.4 Algorithm summary – forward direction

It is beneficial to see the steps of the algorithm to simulate the forward direction summarized as a sort of pseudo-code. Let the number of spatial steps comprising the length of the medium be denoted M_z, and let the number of temporal steps to take in the forward direction be $M_{t\mathrm{f}}$. Assuming that all physical quantities are appropriately defined, the algorithm can be summarized as:

1. Initialize atomic polarizations: Set $\bar{\sigma}_\mathrm{f}(\xi_i,\tau_0,\Delta_k) = 0$ for each i and k
2. Initialize input pulse: Set $\bar{\Omega}_\mathrm{f}(\xi_0,\tau_j) = \Omega_\mathrm{f}[0, t(\tau_j)]$ for each j
3. Define detuning distribution: Set $g(\Delta_k)$ for each k

4. Set loop variable $i = 0$

   (a) Set loop variable $j = 1$

   (b) Calculate $\bar{\sigma}_{\mathrm{f}}(\xi_i, \tau_j, \Delta_k)$ for each k from (5.13)

   (c) Calculate $\delta\Omega(\xi_i, \tau_j)$ using (5.15) and then $\bar{\Omega}_{\mathrm{f}}(\xi_{i+1}, \tau_j)$ with (5.17)

   (d) Increment j

   (e) If $j < M_t$, repeat from (a)

5. Increment i

6. If $i < M_z$, repeat from 4

5.1.5 Simulating the Bloch vector

When simulating $\bar{\mathbf{r}}'$, the Bloch vector in the co-moving frame, equations (5.6) must be evolved in time instead of (5.5). This is still achieved with the RK4 algorithm but with 12 coefficients to be calculated, the four specified by (5.12) for each of the three components of the Bloch vector. Written in vector form these coefficients are given by

$$a_{1\alpha} = \delta\tau \left\{ T_{\alpha\beta}(\xi_i, \tau_j, \Delta_k)\bar{r}'_\beta(\xi_i, \tau_j, \Delta_k) - \delta_{\alpha 3}\Gamma_1 \right\} , \tag{5.18a}$$

$$a_{2\alpha} = \delta\tau \left\{ T_{\alpha\beta}(\xi_i, \tau_{j+1/2}, \Delta_k) \left[\bar{r}'_\beta(\xi_i, \tau_j, \Delta_k) + \frac{1}{2}a_{1\alpha} \right] - \delta_{\alpha 3}\Gamma_1 \right\} , \tag{5.18b}$$

$$a_{3\alpha} = \delta\tau \left\{ T_{\alpha\beta}(\xi_i, \tau_{j+1/2}, \Delta_k) \left[\bar{r}'_\beta(\xi_i, \tau_j, \Delta_k) + \frac{1}{2}a_{2\alpha} \right] - \delta_{\alpha 3}\Gamma_1 \right\} , \tag{5.18c}$$

$$a_{4\alpha} = \delta\tau \left\{ T_{\alpha\beta}(\xi_i, \tau_{j+1/2}, \Delta_k) \left[\bar{r}'_\beta(\xi_i, \tau_j, \Delta_k) + a_{3\alpha} \right] - \delta_{\alpha 3}\Gamma_1 \right\} . \tag{5.18d}$$

Here α and β are indices that run over $\{1, 2, 3\}$, and $\delta_{\alpha\beta}$ is the Kronecker delta. Summation over repeated indices is assumed, and the matrix $\mathsf{T} = T_{\alpha\beta}$ is given by

$$\mathsf{T}(\xi_i, \tau_j, \Delta_k) = \begin{pmatrix} -\Gamma_2 & \Delta_k & 0 \\ -\Delta_k & -\Gamma_2 & \bar{\Omega}_{\mathrm{f}}(\xi_i, \tau_j) \\ 0 & -\bar{\Omega}_{\mathrm{f}}(\xi_i, \tau_j) & -\Gamma_1 \end{pmatrix} . \tag{5.19}$$

As before, the Bloch vector is then evolved via

$$\bar{r}'_\alpha(\xi_i, \tau_{j+1}, \Delta_k) = \bar{r}'_\alpha(\xi_i, \tau_j, \Delta_k) + \frac{a_{1\alpha} + 2a_{2\alpha} + 2a_{3\alpha} + a_{4\alpha}}{6} \ , \tag{5.20}$$

and the integral in the source term of the paraxial wave equation is approximated as

$$\begin{aligned} &\int_{-\infty}^{\infty} \mathrm{d}\Delta \, g(\Delta) \left[\bar{r}'_1(\xi_i, \tau_j, \Delta) - \mathrm{i}\bar{r}'_2(\xi_i, \tau_j, \Delta)\right] \\ &\qquad \approx \sum_k \delta\Delta \, g(\Delta_k) \left[\bar{r}'_1(\xi_i, \tau_j, \Delta_k) - \mathrm{i}\bar{r}'_2(\xi_i, \tau_j, \Delta_k)\right] =: \delta\Omega(\xi_i, \tau_j) \ , \end{aligned} \tag{5.21}$$

In order to simulate the evolution of the Bloch vector instead of the atomic polarization, there are only two modifications that must be made to the algorithm presented in Subsection 5.1.4. One is to calculate $\bar{\mathbf{r}}'$ instead of $\bar{\sigma}_\mathrm{f}$ in Step (b), and the other to calculate $\delta\Omega$ from (5.21) instead of from (5.15) in Step (c).

5.2 Backward-propagating Maxwell-Bloch simulation

The algorithm described in the previous section simulates the absorption by the medium of an incoming (i.e. forward-moving) light pulse. In order to simulate the entire CRIB protocol, it is necessary to use the final state of the medium after the absorption process as the initial state for a wave propagating in the backward direction. This can be achieved with the same sort of algorithm as employed in the previous section, but in the backward-moving reference frame defined by $\xi = z$ and $\tau = t + nz/c$. As in (5.7) the paraxial wave operator in this new frame is given by

$$\frac{n}{c}\partial_t - \partial_z = -\partial_\xi \ , \tag{5.22}$$

while the time derivative is unchanged, $\partial_t = \partial_\tau$. This means that the evolution equations for $\bar{\sigma}$ and $\bar{\mathbf{r}}'$ also remain unchanged; there is however a slight difference to the paraxial wave equation (5.9a) that now has a negative sign on the source term,

$$\partial_\xi \bar{\Omega}_\mathrm{b}(\xi, \tau) = -\mathrm{i}\beta \int_{-\infty}^{\infty} \mathrm{d}\Delta \, g(\Delta) \bar{\sigma}_\mathrm{b}(\xi, \tau, \Delta) \ . \tag{5.23}$$

However, the simulation is now evolving the field in the backward direction so that when its value is known at position ξ_i, the next position at which it must be found is ξ_{i-1} as opposed to ξ_{i+1}. Thus when Newton's quotient is expressed as

$$\partial_\xi \bar{\Omega}_\mathrm{b}(\xi_i, \tau_j) \approx \frac{\bar{\Omega}_\mathrm{b}(\xi_i, \tau_j) - \bar{\Omega}_\mathrm{b}(\xi_{i-1}, \tau_j)}{\delta\xi} \ , \tag{5.24}$$

the unknown value of the field is found as

$$\bar{\Omega}_\mathrm{b}(\xi_{i-1}, \tau_j) = \bar{\Omega}_\mathrm{b}(\xi_i, \tau_j) + \mathrm{i}\beta\, \delta\xi\, \delta\Omega(\xi_i, \tau_j) \ . \tag{5.25}$$

Note that despite the opposite signs in the source terms of the forward- and backward-propagating equations (5.9a) and (5.23), the terms used to calculate the next step of $\bar{\Omega}$, provided by the right-hand sides of (5.17) and (5.25), are the same in either case.

5.2.1 Algorithm summary – backward direction

Since the point of simulating the backward direction is to recall the pulse already stored by the forward simulation, it is assumed that the algorithm in Subsection 5.1.4 has already been run. With that in mind, let $M_{t\mathrm{b}}$ be the total number of time steps in the whole simulation, i.e. $M_{t\mathrm{f}}$ plus the number of time steps to take in the backward direction. In this case, the simulation of the backward direction can be summarized as follows:

1. Initialize polarizations: Set $\bar{\sigma}_\mathrm{b}(\xi_i, \tau_{M_{t\mathrm{f}}}, \Delta_k) = \bar{\sigma}_\mathrm{f}(\xi_i, \tau_{M_{t\mathrm{f}}}, \Delta_k)$ for each i and k
2. Initialize field at end of medium: Set $\bar{\Omega}_\mathrm{f}(\xi_{M_z}, \tau_j) = 0$ for each j
3. Reverse detunings: Set $\Delta_k := -\Delta_k$ for each k
4. Set position loop variable $i = M_z$
   (a) Set time loop variable $j = M_{t\mathrm{f}} + 1$
   (b) Calculate $\bar{\sigma}_\mathrm{b}(\xi_i, \tau_j, \Delta_k)$ for each k from (5.13), with 'b' subscripts replacing 'f'

(c) Calculate $\delta\Omega(\xi_i, \tau_j)$ from (5.15) with 'b' subscripts, and $\bar{\Omega}_{\mathrm{b}}(\xi_{i-1}, \tau_j)$ with (5.25)

(d) Increment j

(e) If $j < M_{t\mathrm{b}}$, repeat from (a)

5. Decrement i

6. If $i > 0$, repeat from 4

5.3 Simulating the protocol

The methods of simulating the evolution of an electric field in a polarizable medium described in the previous two sections can be combined to simulate various forms of the CRIB protocol. There is an inherent limitation to them that must always be kept in mind though: there cannot be in the medium both a forward- and backward-moving field simultaneously. This does not inhibit simulation of either the standard protocol or the modified version defined in this work, yet being aware of it is important none the less.

The methods of the previous sections were used to create the MATLAB code found in Appendix A, which consists primarily of the forward algorithm in Subsection 5.1.4 followed by the backward one of Subsection 5.2.1, along with some commands to visualize the results. In order to be able to simulate the double-recall CRIB protocol the forward-direction algorithm must simulate a longer period of time for one part of the medium than for the rest, which makes the code found in Appendix A slightly more complicated than merely running Subsections 5.1.4 and 5.2.1 sequentially. The general form however is as presented therein.

The simulation allows the user to specify in the code the value of b from the target state (4.30), and from that use (4.34) to calculate the appropriate value of z_0 for the

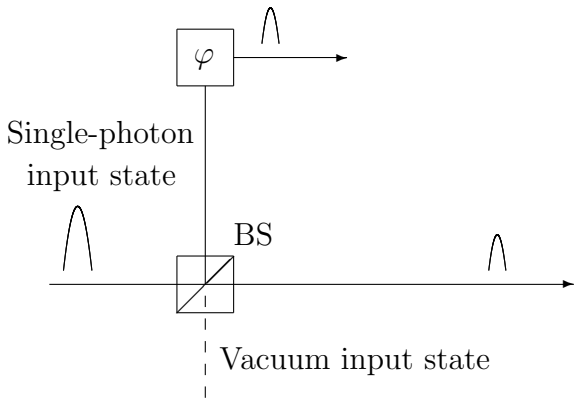

Figure 5.3: The standard method of creating an arbitrary output state $a|0\rangle + be^{i\varphi}|1\rangle$. The state $|0\rangle$ corresponds to the spatial mode transmitted by the variable beam splitter (BS), while $|1\rangle$ corresponds to the reflected mode. The required coupling ratio of the beam splitter is determined by the ratio of a and b.

output state to be $\sqrt{1-b^2}|0\rangle + b|1\rangle$. Note that the simulation results are in the co-rotating, co-moving frame. This means that they do not provide the arbitrary phase differences between the two output pulses described in Chapter 4. Minor changes were made at various points in the code when simulating, for example, multiple input pulses, or creating different visualizations to emphasize the various results; these variations are not included in the appendix.

5.3.1 Example simulation – creating two conjugate bases

With a variable beam-splitter, a phase shifter, and a photon in a single time bin, one can transform a single input pulse into an arbitrary superposition of two spatial modes using the configuration found in Figure 5.3. If one of the spatial modes is delayed and then the two are recombined with an optical switch, the state is transformed into a time-bin qubit. The same situation can be achieved using the double-recall CRIB protocol, as already discussed. Figure 5.4 presents some simulated results showing this; in three different runs a single input pulse in the state $|0\rangle$ has been stored for 100 ns and then recalled as $|0\rangle$, $|1\rangle$, and $(|0\rangle + |1\rangle)/\sqrt{2}$. In the three-dimensional plots the first pulse, from 0 to 50

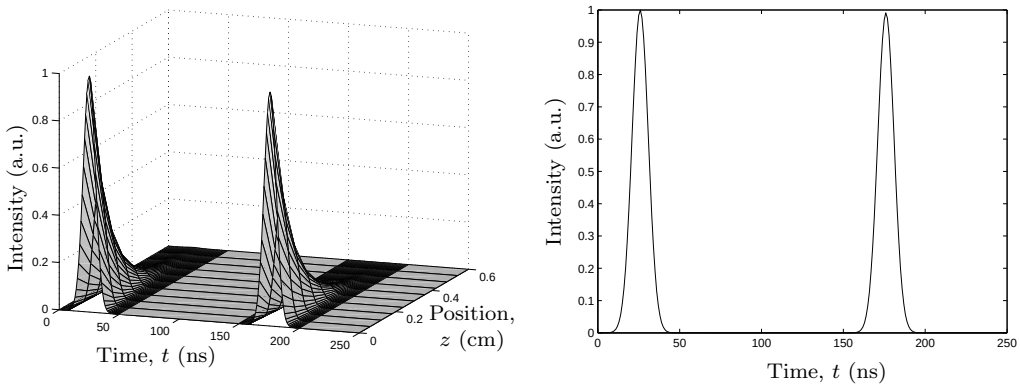

(a) Recalling the input pulse in the state $|0\rangle$

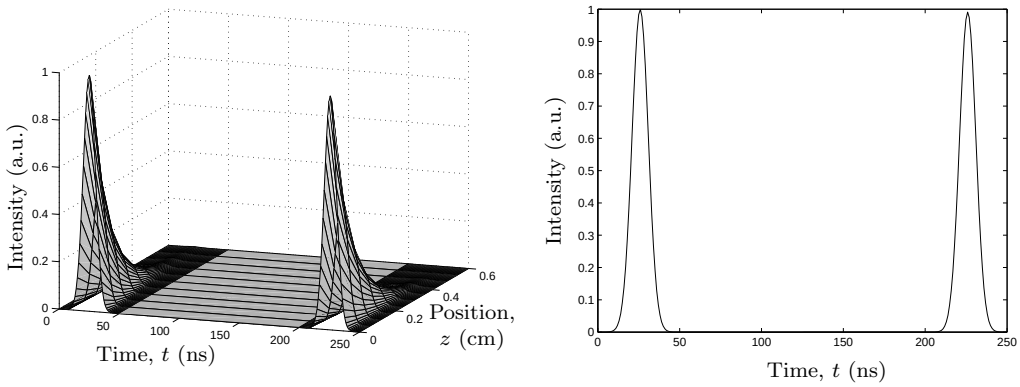

(b) Recalling the input pulse in the state $|1\rangle$

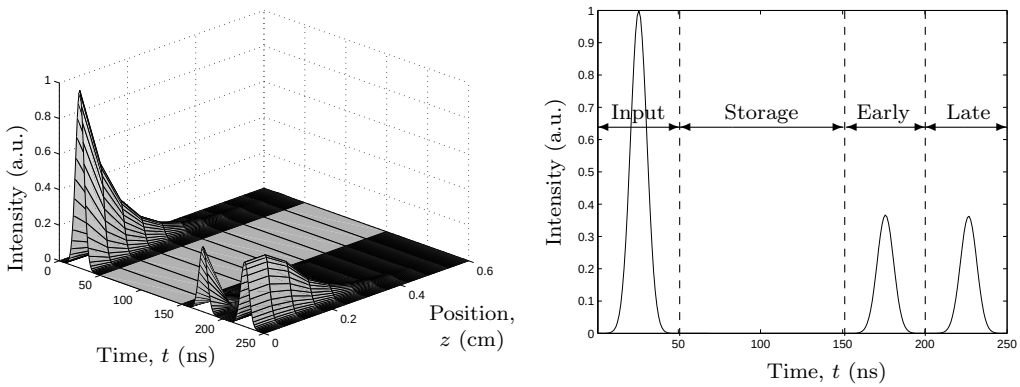

(c) Recalling the input pulse in the superposition state $\frac{1}{\sqrt{2}}(|0\rangle + |1\rangle)$

Figure 5.4: Simulating the transformation of a single input pulse in the state $|0\rangle = |\text{early}\rangle$ into various output states, using the double-recall CRIB scheme. In each case an input pulse centred at $t = 25$ ns propagating in the $+z$ direction is absorbed. (a) Recall was initiated from the entire medium at $t = 100$ ns. (b) Recall was initiated from the entire medium at $t = 125$ ns. (c) Recall began in segment A from $z = 0$ to $z = z_0 = 0.967$ mm at time $t = 100$ ns, and started in the rest of the medium at $t = 125$ ns.

ns, is the input field propagating into and being absorbed by the medium that is 6 mm long. The light is stored during the period of time from 50 ns to either 150 ns or 200 ns, depending on the simulation. The pulses after $t = 150$ ns are those recalled from the medium. Propagating in the negative z direction, they are seen to build up within the medium before exiting it at $z = 0$. Note that the second output pulse in Figure 5.4(c) builds up for a while and then remains constant in amplitude. This starts at the point that the pulse reaches z_0, and is due to the absorption coefficient being negligible in the first segment at that time.

5.3.2 Interfering two time bins

When working with time-bin qubits, one of course cannot always assume that the input to a system will be in a single time-bin state. Indeed, it is the ability to have superpositions of early and late that allows the BB84 protocol to function in the time-bin basis. An important aspect of BB84 implementations in particular, and qubit manipulations in general, is the ability to interfere the portions of the photon in different time bins with each other. Traditionally this is achieved with an unbalanced interferometer, as was seen in Figure 1.2. With the double-recall CRIB protocol this overlap can also be seen by timing the recalls appropriately. If the late time bin recalled from segment A coincides with the early time bin from B, the two fields will be superposed at the memory's output. When the phase difference between the two input pulses is zero, as for the state $|+\rangle$, the two will interfere contructively in the central time bin. On the other hand, a phase difference of π results in destructive interference so that no energy is recalled during the middle time window. These two statements are easily seen in the simulation results presented in Figure 5.5.

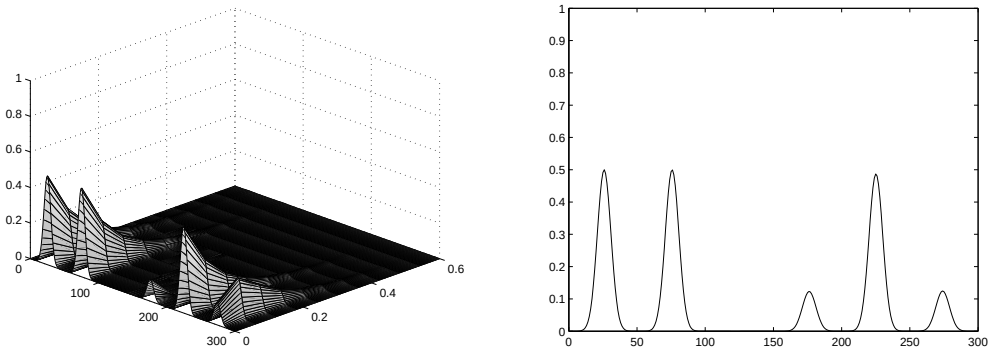

(a) Input state: $|+\rangle$

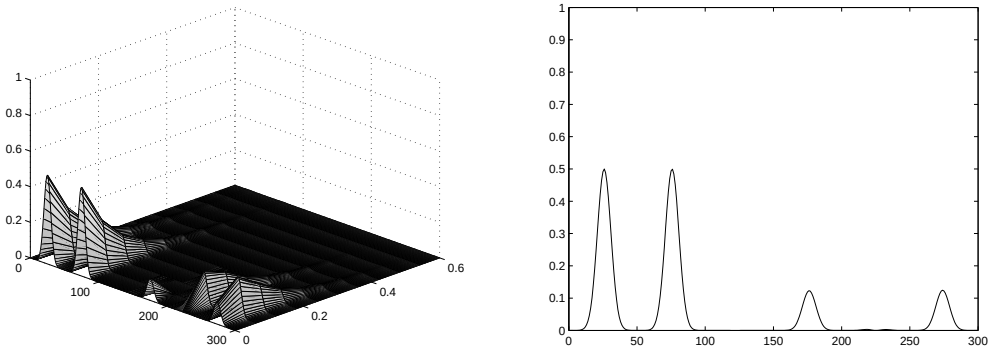

(b) Input state: $|-\rangle$

Figure 5.5: When the input pulse is in a superposition of two time-bin states, recall can be timed such that the two input pulses overlap in the output. This can result in (a) constructive or (b) destructive interference.

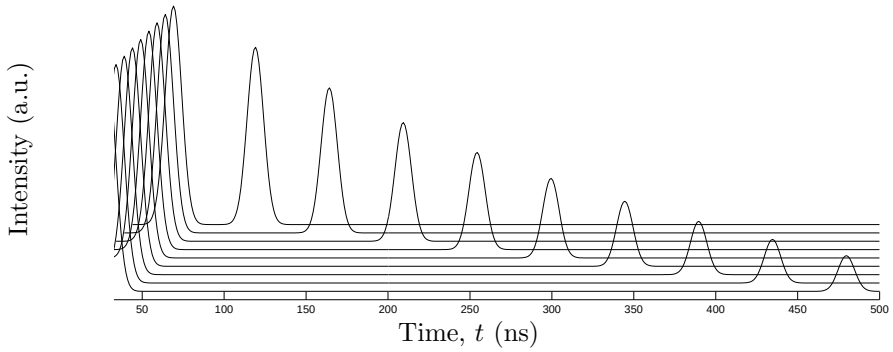

Figure 5.6: The effect of non-zero Γ_2 on recall efficiency. The same input pulse is sent into the medium multiple times, and recalled after various delays. The effect of $\Gamma_2 = 2 \times 10^6$ s^{-1} is easily seen in the decreasing amplitude of the recalled pulses with increasing storage time.

5.3.3 Simulating decoherence

The expected result for a non-zero rate of decoherence is for the efficiency of the recall to decrease exponentially with increased storage time. The simulations were written to include a constant Γ_2 in the evolution of the atomic polarization, but set equal to zero by default. To demonstrate the effect of decoherence, a simulation of the same system was run repeatedly, changing only the recall time for each run. These results can be found in Figure 5.6. It can be seen that the pulse width is unaffected, resulting in a reshaping of the pulse.

To achieve such an obvious decay in the pulse height over less than a microsecond, the decoherence rate was set to $\Gamma_2 = 2 \times 10^6$ s^{-1}. Such a large rate would have a significant impact on the output of the double recall scheme, however at the more physical rate of $\Gamma_2 = 10^5$ s^{-1} the effects of decoherence are negligible over a few tenths of a microsecond. As can be seen in Figure 5.7, the efficiency of the double recall scheme is practically unaffected by the lower decoherence rate, whereas not only is the overall efficiency greatly decreased with the higher rate but the two output pulses are no longer equal in amplitude.

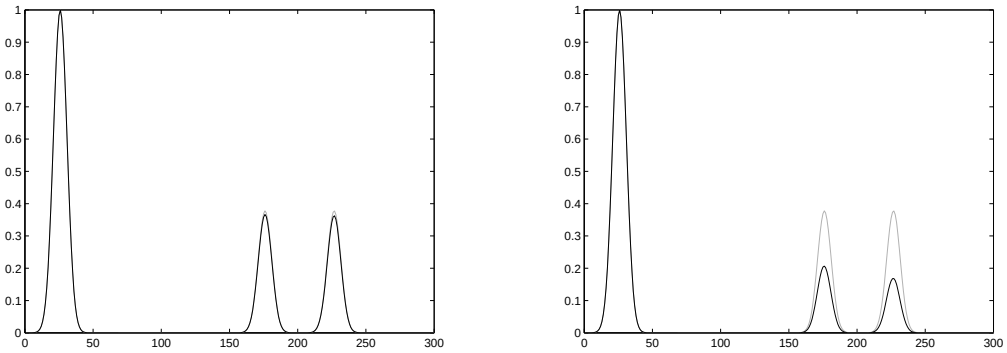

(a) Decoherence rate $\Gamma_2 = 10^5$ s^{-1} (b) Decoherence rate $\Gamma_2 = 2 \times 10^6$ s^{-1}

Figure 5.7: In both plots the results of the ideal ($\Gamma_2 = 0$) case is shown as a lighter line. (a) The total output energy in the case of $\Gamma_2 = 10^5$ s^{-1} is over 96.5% of the recall in the lossless case. (b) The recalled energy with rapid decoherence is less than 50% of the ideal case.

5.3.4 Recall in the forward direction

A user-definable parameter in the code, `fwdSim`, determines whether or not the simulation will recall the pulse in the forward direction. When this boolean variable is true, the entire simulation is run in the forward direction. Figure 5.8 shows the results of two such simulations. In the first, the whole medium was recalled at a single time, with $b = 0$. In this simulation the parameters were set the same as in the creation of Figure 5.4(a). The amplitude of the output pulse within the medium is proportional to $z^2 \mathrm{e}^{-z}$, as predicted by Sangouard *et al.* [SSAG07]. The shape of this predicted curve can be seen in the amplitude of the output pulse of Figure 5.8(a).

In the second simulation, z_0 was calculated so that b would have been $1/\sqrt{2}$ had the recall been in the backward direction. This run used the same parameters as the double-recall simulation presented in 5.4(c). It can be seen that the amplitude of the second output pulse follows the same general shape as the one in Figure 5.8(a). For the length of segment A, i.e. from 0 to z_0, the first output pulse does as well. However, as soon as it enters segment B it starts to get re-absorbed, and decays exponentially

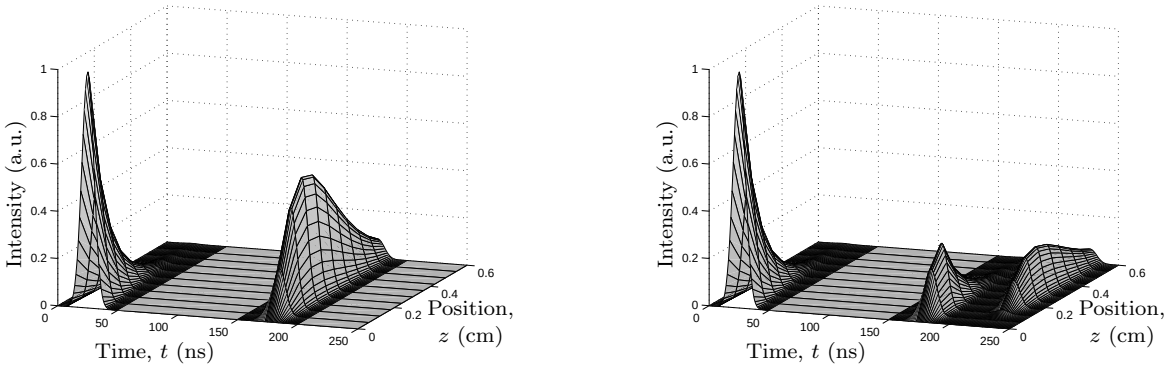

(a) Single recall in the forward direction

(b) Double recall in the forward direction

Figure 5.8: Without application of the $2kz$ phase shift, the pulse continues to travel in the positive z direction when it is recalled. The recalled pulses can be seen to start increasing in amplitude, before continuing to be absorbed by the medium. Besides not switching to the backward direction after storage, all other simulation parameters are the same as those used to create Figure 5.4.

so that there is only negligible output from segment A at $z = L$. This effect can be minimized using the same technique as was used to maximize the output efficiency of the backward-direction double recall. If the pulse is instead recalled from segment B first, after which the absorption coefficient in that region is made as small as possible, then when segment A is recalled its output will move through B unhindered. An example resulting from this setup can be seen in Figure 5.9. While the total energy recalled from the medium is greater than either case in Figure 5.8, it is still less than the output of the double-recall backward case of Figure 5.4(c). Furthermore, some of the original energy is lost due to incomplete absorption of the initial pulse; if the medium is optically dense enough to absorb the entire input, then it will also re-absorb a significant portion of the output.

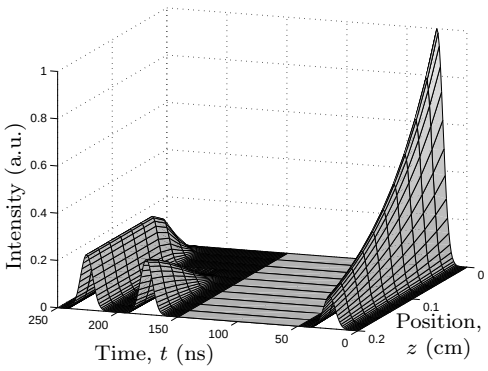

(a) Intensity within the medium. Note that the viewing angle is different from previous plots.

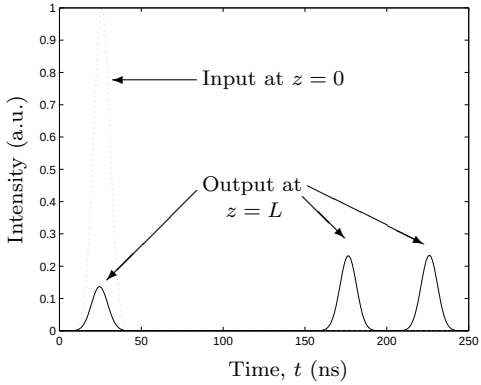

(b) Plot of the pulse intensity at the two ends of the medium.

Figure 5.9: Simulation results for implementing the double-recall protocol in the forward direction with no absorption of the pulse recalled from segment A as it moves through segment B. Note that in order for the important features of the three-dimensional plot of intensity to be visible, this plot views the result from a different angle than previous results; time increases to the left, and the pulse enters at the back and propagates toward the front.

Chapter 6

Concluding remarks

The primary motivation for the present work came from the field of quantum key distribution, in which quantum memory devices are important for extending arbitrarily the distance over which QKD can be performed; in this work a new variation to the well-known quantum memory protocol based on controlled reversible inhomogeneous broadening has been introduced. By treating the storage medium as two separate regions, and by tailoring the relative lengths of those two sections as well as the times at which recall is performed in each one, a method has been constructed that allows quantum state storage to be combined with a beam-splitting operation. For instance, this combination allows the transformation of a single temporally localized pulse into an arbitrary superposition of pulses in two distinct time bins. The double-recall scheme allows this transformation to be performed with nothing more than control of static electric fields, making the method potentially more stable and simple to implement than the current alternative provided by interferometers that must be mechanically stabilized to within a small fraction of an optical wavelength. Of particular importance in the context of experimental QKD is the fact that this allows the performance of projection measurements onto the bases $\mathcal{B}_0$ and $\mathcal{B}_+$, without the need for interferometers to be stabilized over long distances. Important steps toward this result have been made, as seen in the results of Figure 5.5 that show constructive and destructive interference at the output of the medium. This corresponds to one of the output ports of an interferometer. Future directions for expanding the scope of this work include an investigation into methods for reproducing the results of the second output port in order to complete the set of measurements required by BB84. This will provide another use of quantum memory within the realm of QKD.

Appendix A

MATLAB simulation code

The simulation results presented in Chapter 5 were created with the code listed below, with modification only to parameters as mentioned in the text or to the visualization commands employed at the end.

```
%%%%%%%%%%%%%%%%%%%%%%%%%%%%%%%%%%%%%%%%%%%%%%%%%%%%%%%%%%%%%%%%%%%%%%%%%%%%

display([datestr(now,14), ': Initializing']);

clear all;
close all;

opengl neverselect; % Solves some graphics-card related crashes

%% Options

fwdSim = false;

b=1/sqrt(2); % Probability amplitude of second output pulse

% All quantities are defined in SI units
tDuration = 300e-9; % Duration of simulation, 300 ns
L = 0.006;          % Length of simulated medium, 6 mm

tau = 10e-9;  % Temporal width of pulse, 10 ns
wL = 4.77e13; % Central frequency of laser
              % Corresponds to 1000 nm wavelength

tp = 25e-9;  % Centre of pulse, 25 ns
binSep = 50e-9;
TA = 100e-9; % Time when recall starts in segment A
TB = 125e-9; % Time when recall starts in segment B

gam = 1e9; % Storage bandwidth of medium, 1 GHz

nr = 1.5;         % refractive index of medium
c = 299792458;    % speed of light
hb = 1.05457e-34; % reduced Planck's constant, hbar
mu0 = pi*4e-7;    % permeability of free space
```

```
ep0 = 8.854e-12;  % permittivity of free space
N = 1e25;         % Number density of absorbers in the medium
p = 1.67e-32;     % Dipole moment
Gam2 = 10^5;      % Decoherence rate
beamWidth = 4e-3; % 4 mm

polinit = 0.0; % Initial polarization of atoms
               % 0 => all in ground state

% Define array sizes
numTimes = 300;
numZeds = 1000;
numDeltas = 100;

%% Derived quantities

tStart = 0;
tEnd = tStart+tDuration;

zStart = 0;
zEnd = zStart+L;

kL = nr*wL/c;
E0 = sqrt(hb*wL*sqrt(2/pi^3)/(ep0*c*tau*beamWidth^2));

% Calculate time, distance, and frequency step sizes
dt = tDuration/(numTimes-1);
dz = L/(numZeds-1);
dD = gam/(numDeltas-1);

% Calculate coupling strength and absorption coefficient
beta = wL*N*p^2/(2*ep0*hb*nr*c);
alpha = 2*beta*pi/gam;

% If b is 0, z0 should be infinite (i.e. equal to
% the assumed value of L); this gives problems to
% the Matlab routine that finds the array element
% of zeds closest to z0 - so fill it in manually.
if b==0
    z0 = L;
else
    z0 = acosh((1+b^2)/(2*b^2))/alpha;
end;
```

```
%% Initial conditions

% Create arrays to hold real-world times and positions
times = tStart:dt:tEnd;
zeds = zStart:dz:zEnd;
% Initialize the field to zero everywhere in the simulation domain
Omega = zeros(numZeds,numTimes);

% Define a Gaussian input pulse centred at tp
pulseTimes1 = times - tp;
pulseTimes2 = times - (tp+binSep);
Omega(1,:) = E0*exp(-pulseTimes1.*pulseTimes1/tau^2);

% Define the initial and reversed detunings
posDeltas = (-gam/2):dD:(gam/2);
negDeltas = -posDeltas;

% Create the detuning distribution g(Delta)
g = ones(1,numDeltas)/gam;


%% Find the array elements closest to the desired times and positions

[minDiff, tSwitchA] = min(abs(times-TA));
[minDiff, tSwitchB] = min(abs(times-TB));
[minDiff, zSplit] = min(abs(zeds-z0));

Tm = TA+TB-tp;
[minDiff, tMidPoint] = min(abs(times-Tm));


%% The simulation itself

% An array to save the atomic states after the forward simulation
polsave = zeros(numZeds,numDeltas);

Deltas = posDeltas;

for n=1:numZeds

    % Initialize the polarizations at this position
    pol = polinit*ones(1,numDeltas);

    % The field at the first time step won't change, unless polarization
```

```
% exists in the medium before the field arrives
if n<numZeds;
    %Note that this does nothing in the normal case of polinit=0
    dE = i*beta*dD*sum(g.*pol);
    Omega(n+1,1) = Omega(n,1) + dE*dz;
end;

% In the section A the detunings are switched at a different time
% than in section B
if n<zSplit
    runTime = tSwitchA-1;
else
    runTime = tSwitchB-1;
end;


for s=1:runTime

    % Determine the current, next, and intermediate values of the
    % electric field, needed by the RK4 algorithm
    Om = Omega(n,s);
    OmNext = Omega(n,s+1);
    OmHalf = (Om+OmNext)/2;

    % Find the RK coefficients
    k1 = dt*((i*Deltas-Gam2).*pol + i*Om);
    k2 = dt*((i*Deltas-Gam2).*(pol+k1/2) + i*OmHalf);
    k3 = dt*((i*Deltas-Gam2).*(pol+k2/2) + i*OmHalf);
    k4 = dt*((i*Deltas-Gam2).*(pol+k3) + i*OmNext);

    % Calculate pol(n,s+1) using RK4
    pol = pol + (k1 + 2*k2 + 2*k3 + k4)/6;

    % Calculate the change in Omega over the next step
    dOm = i*beta*dD*sum(g.*pol);

    if n<numZeds
        Omega(n+1,s+1) = Omega(n,s+1) + dOm*dz;
    end;

end; % s-loop (times)

% Save the polarizations at time tSwitchA or tSwitchB
polsave(n,:) = pol;
```

```
    % Print a status update occasionally
    if mod(n,numZeds/10)==0; display(['z=',num2str(n)]); end;
end;

% Setup variables that allow the next section of code to
% work in either the forward or backward direction
if fwdSim
    first = 1;
    last = numZeds;
    inc = 1;
else
    first = numZeds;
    last = 1;
    inc = -1;
end;

% Reverse the detunings
Deltas = negDeltas;

% Continue the simulation, in the appropriate direction
for n=first:inc:last

    % Restore the polarization state at the current position
    % from the the result of the above simulation
    pol = polsave(n,:);

    % The start time for the current simulation, as well as the order
    % in which sections are made transparent, depend on the simulation
    % direction.
    if n<zSplit
        runTime = tSwitchA;
        if fwdSim
            betaSec2 = beta;
        else
            betaSec2 = 0;
        end;
    else
        runTime = tSwitchB;
        if fwdSim
            betaSec2 = 0;
        else
            betaSec2 = beta;
        end;
```

```
    end;

    if n ~= last;
        dE = i*beta*dD*sum(g.*pol);
        Omega(n+inc,runTime) = Omega(n,runTime) + dE*dz;
    end;

    betaUse = beta; % Restore the original value of beta,
                    % in case 0 was used in the previous interation

    for s=runTime:numTimes-1

        if s==tMidPoint
            betaUse = betaSec2;
        end;

        Om = Omega(n,s); %*2*p/hb;
        OmNext = Omega(n,s+1); %*2*p/hb;
        OmHalf = (Om+OmNext)/2;

        k1 = dt*((i*Deltas-Gam2).*pol + i*Om);
        k2 = dt*((i*Deltas-Gam2).*(pol+k1/2) + i*OmHalf);
        k3 = dt*((i*Deltas-Gam2).*(pol+k2/2) + i*OmHalf);
        k4 = dt*((i*Deltas-Gam2).*(pol+k3) + i*OmNext);

        pol = pol + (k1 + 2*k2 + 2*k3 + k4)/6;

        dOm = i*betaUse*dD*sum(g.*pol);

        if n ~= last;
            Omega(n+inc,s+1) = Omega(n,s+1) + dOm*dz;
        end;

    end; % s-loop (times)

    if mod(n,numZeds/10)==0; display(['z=',num2str(n)]); end;
end;

display([datestr(now,14), ': Finished simulation']);

% The complex field cannot be easily visualized,
% and intensity is what is measured experimentally.
% So, calculated the normalized (to one E0 photon)
% intensity of the field.
```

```
intens = Omega.*conj(Omega)/E0^2;

% Visualize the result as a surface plot
figure;
surf(10^9*times([1:50 150:250]), ...
     100*zeds([1:100:numZeds numZeds]), ...
     intens([1:100:numZeds numZeds],[1:50 150:250]));
numShades = 16;
gryMap = linspace(0.7,0.9,numShades);
colormap([gryMap; gryMap; gryMap]');
view([45 30]);
set(gca,'YLim',[0,100*L]);
set(gca,'ZLim',[0,1]);

% Visualize the input and output from the medium at z=0
figure;
plot(intens(1,:),'-k');
set(gca,'YLim',[0,1]);
set(gca,'XLim',[1,250]
);
%%%%%%%%%%%%%%%%%%%%%%%%%%%%%%%%%%%%%%%%%%%%%%%%%%%%%%%%%%%%%%%%%%%%%%%%%%%%%%%
```

Appendix B

Notations and symbols used

$\|0\rangle$, $\|1\rangle$	computational basis states from Chapter 4 on (see Page 51)
$\|1\rangle$, $\|2\rangle$	ground and excited states of a two-level system (see Page 10)
α	absorption coefficient (see Pages 26 and 30)
β	coupling strength between the atoms and light (see Page 16)
c	speed of light in vacuum, $c = 299792458$ m/s
c.c.	complex conjugate
χ	scaling factor of the recalled field amplitude (see Page 34)
$\partial_{(\cdot)}$	partial derivative with respect to the subscript
Δ	a detuning, $\Delta = \omega_0 - \omega_L$ (see Page 11)
$\delta(\cdot)$	Dirac delta distribution
δt	temporal width of the pulse to be stored (see Page 23)
E	energy in the light pulse (see Page 36)
$\mathbf{E}$	electric field
$\mathcal{E}$	pulse envelope
$\boldsymbol{\varepsilon}$	polarization vector
ϵ_0	permittivity of free space, $\epsilon_0 \approx 8.854 \times 10^{-12}$ C^2/N m^2
η	constant related to decoherence effects (see Page 31)
$g(\Delta)$	distribution of detunings within the medium (see Page 11)
γ	width of absorption profile (see Figure 3.1(c) and Page 3.4)
Γ_2	decoherence rate in the system (see Page 24)
$\hat{H}_A$, $\hat{H}_I$	atomic and interaction Hamiltonians (see Pages 10 and 12)
$\hbar$	reduced Planck's constant, $h/2\pi \approx 1.055 \times 10^{-34}$ J s
i	the complex unit, $\mathrm{i}^2 = -1$
$\mathrm{Im}(\cdot)$	the imaginary part of the argument
k	wavenumber, $k = n\omega_L/c$
L	length of the memory medium (see Page 17)
μ	recall efficiency (see Page 36)
$\boldsymbol{\mu}_{12}$, $\hat{\boldsymbol{\mu}}$	atomic dipole moment and operator (see Page 12)
n	refractive index or a summation index, dictated by context
N	linear density of atomic dipoles (see Page 12)
$\Omega(z,t)$	Rabi frequency corresponding to the light field (see Page 16)
$\tilde{\Omega}(z,\omega)$	Fourier transform of the Rabi frequency
$\bar{\Omega}(\xi,\tau)$	Rabi frequency in the co-moving frame (see Page 57)
ω_0	transition frequency of a two-level system (see Page 11)
ω_L	central frequency of laser light pulse
ODE, PDE	ordinary or partial differential equation
$\mathbf{P}$	polarization of the medium (see Page 12)
$\wp$	projection of light's polarization on the dipole moment (see Page 13)

$\mathbf{r}$, r_i	Bloch vector, its components (see Page 10)
$\mathbf{r}'$, r_i'	Bloch vector and its components in the co-rotating frame (see Page 14)
$\hat{\rho}$, ρ_{ij}	density operator, its components $\rho_{ij} = \langle i\|\hat{\rho}\|j\rangle$
$\mathrm{Re}(\cdot)$	the real part of the argument
σ	atomic polarization (see Page 12)
$\bar{\sigma}$	atomic polarization in co-moving frame (see Page 57)
t	time variable
T_0	time at which CRIB protocol is initiated (see Page 18)
T_2	inverse of the medium's optical linewidth (see Page 23)
T_A, T_B	times at which recall is initiated in segments A and B
t_p	time of the peak of the input pulse (see Page 23)
U	energy stored in the electric field (see Page 54)
w	cross-sectional width of the light pulse (see Page 54)
z	position variable
z_0	point between $z = 0$ and $z = L$ at which the memory is split

References

[AEW+05] A. André, M. D. Eisaman, R. L. Walsworth, A. S. Zibrov, and M. D. Lukin. Quantum control of light using electromagnetically induced transparency. *Journal of Physics B*, 38:S589–S604, 2005.

[AFK+08] Jürgen Appel, Eden Figueroa, Dmitry Korystov, M. Lobino, and A. I. Lvovsky. Quantum memory for squeezed light. *Phys. Rev. Lett.*, 100:093602, 2008.

[AKH66] I. D. Abella, N. A. Kurnit, and S. R. Hartmann. Photon echoes. *Phys. Rev.*, 141(1):391 – 406, January 1966.

[Ale07] Annabel Lucy Alexander. *Investigation of Quantum Information Storage in Rare Earth Doped Materials*. PhD thesis, Australian National University, March 2007.

[ALSM06] A. L. Alexander, J. J. Longdell, M. J. Sellars, and N. B. Manson. Photon echoes produced by switching electric fields. *Phys. Rev. Lett.*, 96:043602, February 2006.

[AML06] Jürgen Appel, K.-P. Marzlin, and A. I. Lvovsky. Raman adiabatic transfer of optical states in multilevel atoms. *Phys. Rev. A*, 73:013804, January 2006.

[BB84] C. H. Bennett and G. Brassard. Quantum cryptography: Public key distribution and coin tossing. In *Proceedings of IEEE International Conference on Computers, Systems and Signal Processing*, pages 175–179, December 1984.

[BB89] Charles H. Bennett and Gilles Brassard. The dawn of a new era in quantum cryptography: The experimental prototype is working! *SIGACT News*, 20:78–83, 1989.

[BBB+92] Charles H. Bennett, François Bessette, Gilles Brassard, Louis Salvail, and John Smolin. Experimental quantum cryptography. *Journal of Cryptology*, 5(1):3–28, January 1992.

[BBE92] C. H. Bennett, G. Brassard, and A. K. Ekert. Quantum cryptography. *Scientific American*, 267:50–57, October 1992.

[BBM+07] A. D. Boozer, A. Boca, R. Miller, T. E. Northup, and H. J. Kimble. Reversible state transfer between light and a single trapped atom. *Phys. Rev. Lett.*, 98:193601, May 2007.

[BDCZ98] H.-J. Briegel, W. Dür, J. I. Cirac, and P. Zoller. Quantum repeaters: The role of imperfect local operations in quantum communication. *Phys. Rev. Lett.*, 81(26):5932–5935, December 1998.

[BGTZ99] J. Brendel, N. Gisin, W. Tittel, and H. Zbinden. Pulsed energy-time entangled twin-photon source for quantum communication. *Phys. Rev. Lett.*, 82(12):2594–2597, March 1999.

[BIH91] K.-J. Boller, A. Imamoğlu, and S. E. Harris. Observation of electromagnetically induced transparency. *Phys. Rev. Lett.*, 66(20):2593–2596, May 1991.

[Blo46] F. Bloch. Nuclear induction. *Phys. Rev.*, 70(7 and 8):460–474, October 1946.

[Cha08] Thierry Chanelière. Quantum storage investigation in thulium based materials. In *Storage and Manipulation of Quantum Information in Optically-Addressed Solids*, January 2008.

[CMJ+05] T. Chanelière, D. N. Matsukevich, S. D. Jenkins, S.-Y. Lan, T. A. B. Kennedy, and A. Kuzmich. Storage and retrieval of single photons transmitted between remote quantum memories. *Nature*, 438:833–836, 2005.

[DLCZ01] L. M. Duan, M. D. Lukin, J. I. Cirac, and P. Zoller. Long-distance quantum communication with atomic ensembles and linear optics. *Nature*, 414:413–418, November 2001.

[Eke91] Artur K. Ekert. Quantum cryptography based on bell's theorem. *Phys. Rev. Lett.*, 67(6):661–663, August 1991.

[EPR35] A. Einstein, B. Podolsky, and N. Rosen. Can quantum-mechanical description of physical reality be considered complete? *Physical Review*, 47:777–780, May 1935.

[FL00] M. Fleischhauer and M. D. Lukin. Dark-state polaritons in electromagnetically induced transparency. *Phys. Rev. Lett.*, 84(22):5094–5097, May 2000.

[HFI90] S. E. Harris, J. E. Field, and A. Imamoğlu. Nonlinear optical processes using electromagnetically induced transparency. *Phys. Rev. Lett.*, 64(10):1107–1110, March 1990.

[HHDB99] Lene Vestergaard Hau, S. E. Harris, Zachary Dutton, and Cyrus H. Behroozi. Light speed reduction to 17 metres per second in an ultracold atomic gas. *Nature*, 397:594–598, 1999.

[HLA+08] G. Hétet, J. J. Longdell, A. L. Alexander, P. K. Lam, and M. J. Sellars. Gradient echo quantum memory for light using two-level atoms. *Phys. Rev. Lett.*, 100:023601, January 2008.

[HSSA+06] Sara R. Hastings-Simon, Matthias U. Staudt, Mikael Afzelius, Pascal Baldi, Didier Jaccard, Wolfgang Tittel, and Nicolas Gisin. Controlled stark shifts in er^{3+}-doped crystalline and amorphous waveguides for quantum state storage. *Optics Communications*, 266(2):716–719, October 2006.

[id 05] id Quantique. *Clavis: Plug & Play Quantum Cryptography,* id 3000 *datasheet*, v2.1 edition, 2005.

[KAH64] N. A. Kurnit, I. D. Abella, and S. R. Hartmann. Observation of a photon echo. *Phys. Rev. Lett.*, 13(19):567–568, November 1964.

[KTG+06] B. Kraus, W. Tittel, N. Gisin, M. Nilsson, S. Kröll, and J. I. Cirac. Quantum memory for nonstationary light fields based on controlled reversible inhomogeneous broadening. *Phys. Rev. A*, 73:020302(R), 2006.

[LB06] Michel Le Bellac. *A Short Introduction to Quantum Information and Quantum Computation*. Cambridge University Press, 2006.

[LDBH01] Chien Liu, Zachary Dutton, Cyrus H. Behroozi, and Lene Vestergaard Hau. Observation of coherent optical information storage in an atomic medium using halted light pulses. *Nature*, 409:490–493, January 2001.

[Mat07] The MathWorks, Inc. MATLAB R2007B: The language of technical computing. Software, 1984-2007.

[Mel05] R. S. Meltzer. *Spectroscopic Properties of Rare Earths in Optical Materials*, chapter 4. Line Broadening Mechanisms and Their Measurement, pages 191–265. Springer Series in Materials Science. Tsunghua University Press and Springer-Verlag, 2005.

[MK01] S. A. Moiseev and S. Kröll. Complete reconstruction of the quantum state of a single-photon wave packet absorbed by a doppler-broadened transition. *Phys. Rev. Lett.*, 87(17):173601, October 2001.

[MW95] Leonard Mandel and Emil Wolf. *Optical Coherence and Quantum Optics*. Cambridge University Press, 1995.

[NC00] Michael A. Nielsen and Isaac L. Chuang. *Quantum Computation and Quantum Information*. Cambridge University Press, 2000.

[NK05] Mattias Nilsson and Stefan Kröll. Solid state quantum memory using complete absorption and re-emission of photons by tailored and externally controlled inhomogeneous absorption profiles. *Optics Communications*, 247:393–403, March 2005.

[PFM+01] D. F. Phillips, A. Fleischhauer, A. Mair, R. L. Walsworth, and M. D. Lukin. Storage of light in atomic vapor. *Phys. Rev. Lett.*, 86:783–786, 2001.

[RZBB94] Michael Reck, Anton Zeilinger, Herbert J. Bernstein, and Philip Bertani. Experimental realization of any discrete unitary operator. *Phys. Rev. Lett.*, 73(1):58–61, July 1994.

[SSAG07] Nicolas Sangouard, Christoph Simon, Mikael Afzelius, and Nicolas Gisin. Analysis of a quantum memory for photons based on controlled reversible inhomogeneous broadening. *Phys. Rev. A*, 75:032327, March 2007.

[Sta08] Matthias Ulrich Staudt. *Probing Coherent Optical Memories in Rare-Earth-Ion-Doped Materials*. PhD thesis, Université de Genève, April 2008.

[STC+02] Y. Sun, C. W. Thiel, R. L. Cone, R. W. Equall, and R. L. Hutcheson. Recent progress in developing new rare earth materials for hole burning and coherent transient applications. *Journal of Luminescence*, 98:281–287, 2002.

[WA04] Hans J. Weber and George B. Arfken. *Essential Mathematical Methods for Physicists*. Elsevier Academic Press, 2004.

[WZ82] W. K. Wootters and W. H. Zurek. A single quantum cannot be cloned. *Nature*, 299:802–803, October 1982.